
Decom-Renorm-Merge: Model Merging on the Right Space Improves Multitasking

Yuatyong Chaichana
Chulalongkorn University

Thanapat Trachu
Chulalongkorn University

Peerat Limkonchotiwat
AI Singapore

Konpat Preechakul
UC Berkeley

Tirasan Khandhawit
Mahidol University

Ekapol Chuangsuwanich *
Chulalongkorn University

Abstract

In the era of large-scale training, model merging has evolved into a tool for creating multitasking models efficiently. It enables the knowledge of models to be fused, without the need for heavy computation as required in traditional multitask learning. Existing merging methods often assume that entries at identical positions in weight matrices serve the same function, enabling straightforward entry-wise comparison and merging. However, this assumption overlooks the complexity of finetuned neural networks, where neurons may develop distinct feature compositions, making direct entry-wise merging problematic. We present **Decom-Renorm-Merge (DRM)**, a simple yet effective approach that leverages Singular Value Decomposition to decompose and coordinate weight matrices into an aligned joint space, where entry-wise merging becomes possible. We showcase the effectiveness of DRM across various settings ranging from smaller encoder-based such as ViT and DeBERTa, encoder-decoder-based such as T5, and larger decoder-based such as Llama3.1-8B. Our experimental results show that DRM outperforms several state-of-the-art merging techniques across full finetuning and low-rank adaptation settings. Moreover, our analysis reveals renormalization as the crucial component for creating a robust and even joint space for merging, significantly contributing to the method’s performance.

1 Introduction

Multitask learning [8] aims to equip machine learning models with the generalist ability of humans—to acquire and perform multiple tasks using a single model. This capability is best demonstrated in large language models [63, 76, 7, 47, 75], which can simultaneously handle a wide range of tasks requiring language understanding. However, acquiring high-quality training data—especially for specialized domains such as medicine, law, or finance—is often constrained by proprietary access, licensing, or privacy concerns. Finding the right task and data mixtures requires costly trial and error [1], where even a single training run can be a major investment. These challenges have motivated research into model merging as an alternative.

Rather than training a multitask model from scratch, model merging combines independently finetuned checkpoints into a single multitask-capable model, without requiring additional training. This also permits the reuse of an increasing number of open-source finetuned models. Ilharco et al. [35] introduces the use of *task vector*—defined as the difference between finetuned and base parameters—as a way to perform various arithmetic operations such as addition for task fusion, and subtraction for task forgetting. Many merging techniques adopt task vectors, since they better capture the finetuning

*Correspondence to ekapol.c@chula.ac.th

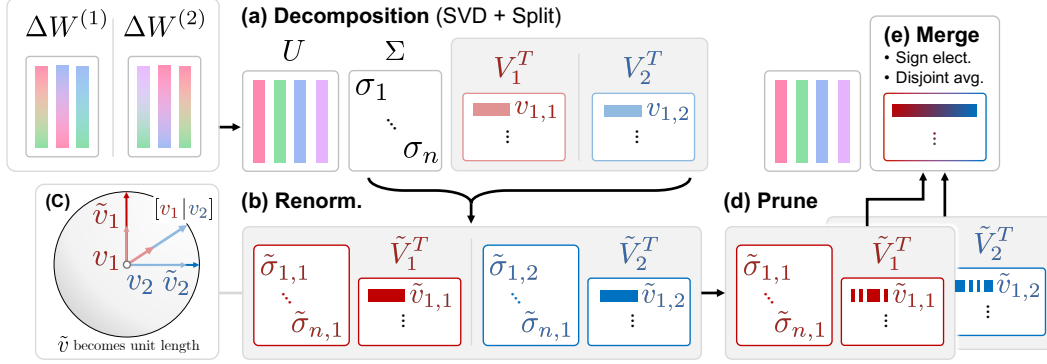


Figure 1: **Decom-Renorm-Merge (DRM)** is a model-merging method for building multitask models. Different models may not share the same weight parameterization. Thus, *merging should occur in a shared decomposed weight space, not the original parameter space*. DRM merges models’ weight deltas $\Delta W^{(t)}$ —the difference of each finetuned model from a shared base model—into a single merged delta. DRM consists of four main steps: **(a) Decompose**: Concatenate the $\Delta W^{(t)}$ matrices horizontally (or vertically), then apply SVD to decompose them into a shared basis U and individual weights V_t . Although the combined V is orthonormal, each individual split V_t is not. **(b) Renormalize** each row vector $v_{t,i}$ of V_t to unit length, and scale the corresponding singular value to preserve the magnitude. This can be viewed as compensating for V_t ’s non-orthonormality as illustrated in (c). **(d) Prune** each renormalized individual singular vector matrix \tilde{V}_t by keeping only the entries within top- $k\%$ magnitudes. **(e) Merge** the pruned singular vector matrices across models using sign election and disjoint averaging.

dynamic and update direction. Furthermore, it is found that a large portion of task vector entries can be pruned without heavily impacting task-specific performance [83]. This sparsity also enhances merging performance by reducing parameter interferences between models.

Parameter interference is identified in TIES Merging [83] as a key obstacle to effective model merging. They demonstrate that two major interferences are redundant parameter values and sign disagreements at corresponding positions in the weight matrices. Yadav et al. [83] propose to address the issue by first pruning small entries from the task vectors. Then, in each position, one dominant sign is selected, and all other entries with opposite sign are zeroed out. The pruned entries are ignored during the final averaging step.

These interference mitigation operations, employed in TIES [83] and its variants [85], rely on a crucial assumption: task vector entries at identical positions serve consistent semantic roles and functions. This assumption allows entry-wise comparison, pruning, dominant sign selection, and the subsequent averaging to be done. However, this fundamental assumption may not hold in practice, as: (a) finetuning can lead to changes in feature arrangement of the activations and (b) a single neuron often carries not just a single, but a composition of several overlapping features, a phenomenon known as polysemanticity [19, 67, 53]. Based on these observations, we formulate our central hypothesis: for entry-wise interference reduction strategies to be valid during model merging, task vectors *must first be decomposed and then coordinated into a shared representation space*.

Following our hypothesis, we propose **Decom-Renorm-Merge (DRM)**, a method that merges models in a shared representation space. Unlike previous approaches that operate on task vectors (task-specific parameter differences flattened into vector form), DRM preserves the matrix structure of updates—referred to as the *weight delta*—which is essential for decomposing into a shared basis. As shown in Figure 1, DRM consists of four key steps: (1) **Decompose** a concatenated set of weight delta matrices using SVD to extract a shared basis and project each model into this joint space. (2) **Renormalize** each model’s projected basis vectors to unit length; this step is crucial for stable merging. (3) **Prune**: Keep only the top magnitude entries in each renormalized basis vector matrix to reduce interference. (4) **Merge**: Combine the pruned weights across models using the rest of TIES’ interference mitigation techniques [83].

We demonstrate the effectiveness of DRM across various setups, including: (1) Diverse model architectures and sizes. Ranging from smaller encoder-based ViT-B/32, ViT-L/14 [15, 61], and DeBERTa-Base [26]; mid-sized, encoder-decoder model T5-Base and T5-Large [63]; to large decoder-

based Llama3.1-8B [24]. (2) Comprehensive task categories and modalities. Including image recognition and natural language understanding. (3) With and without validation set for merging techniques’ hyperparameter tuning. Notably, even with no validation set available, DRM outperforms the strongest baselines by 5.0% and 1.9% in merging ViT-B/32 and ViT-L/14, respectively, 9.3% on DeBERTa-Base-v3, and 1.9% on low-rank (LoRA) adapted Llama3.1-8B, on absolute scales. Additionally, we demonstrate that DRM has better performance retention as the number of tasks being merged increases, compared to other baselines.

Through detailed analysis of the aligned joint merging spaces, we uncover that naively performing interference mitigation and merging operations in the joint space obtained from SVD yields surprisingly minimal improvements. Instead, we identify *renormalization* as the crucial enabling component of our method. The technique involves normalizing the split singular vectors back to unit length after they lose this property due to the splitting. Without this key ingredient, the singular vector bases demonstrate significant instability, leading to an erratic pruning outcome where some top principle components are entirely zeroed out, causing severe performance degradation.

In particular, our work makes the following main contributions:

- We propose **Decom-Renorm-Merge (DRM)**, a novel model merging technique that constructs a shared representation space for more effective model merging.
- We demonstrate **state-of-the-art performance** across both vision and language domains, including CLIP’s vision encoders ViT-B/32 and ViT-L/14, DeBERTa-Large-V3, and LoRA-finetuned LLaMA 3.1-8B, showcasing the effectiveness of our method in both full and parameter-efficient settings.
- We identify and analyze the critical role of renormalization (Section 6) in enabling stable and robust merging within the shared decomposed weight space.

2 Related Works

Model Merging and Weight Combination. Early research on model merging starts by means of averaging together different finetuned weights derived from identical model architectures and tasks, with a goal to improve the final performance of that specific task [81, 36, 25], and generalization ability [5, 9, 65, 64]. Candidate weights for averaging can be obtained either from different optimization steps or entirely different training runs. Choshen et al. [12] show that the averaged weights can be used as a better initialization point for new task finetuning. Merging was later extended to combining weights of different tasks, creating a single multitasking model. Pioneered by Matena and Raffel [50], rather than simply averaging the parameters, the previous work weights the averaging using Fisher information matrices, effectively capturing the importance of each parameter. But the Fisher information has to be calculated from the network’s gradient. Regression Mean [38] frames merging problem as linear regression of each individual linear layer in the model. While a closed-form solution exists, it requires additional activation statistics from the models. Task Arithmetic [35] proposes task vector, which is attained by subtracting the base out from finetuned weight. Inspired by task analogy and regular vector arithmetic, they showcase effectiveness on applying arithmetic operations to the task vectors, such as addition for task merging, and subtraction for task forgetting. [59] introduce a novel linearized finetuning on the tangent plane, in order to facilitate downstream task vector arithmetic. TIES Merging [83] adheres to the use of task vector. They demonstrate that a combination of parameter pruning, and dominant sign election, can resolve parameter interference and significantly enhance merging performance. DARE [85] displays excessive redundancy within task vectors. They propose random parameter pruning and rescaling as remedies, paving the way for other merging methods to be applied effectively afterwards.

Mode Connectivity and Weight Permutation. Even with the complex and highly non-convex nature of the loss surfaces of deep neural networks, it was found that there exists paths, possibly linear, of near-constant low loss between independently optimized large models, a phenomenon called mode connectivity [22, 23, 16, 21]. Based on these findings, a body of works [20, 74] argue the probable existence of weight permutation symmetry in neural network. Namely, two differently trained models can be permuted and aligned into a same convex basin, in which there is a linearly interconnecting path. This subsequently allows the permuted networks to be merged simply via weight averaging [69, 48, 3, 39, 60, 72].

3 Motivation: Merging models on the right space

Problem settings. Our goal is to merge several finetuned models, each derived from the same pretrained base, into a single multitask model while maintaining maximum performance across all merged tasks, without involving any forward-backward calculation or architectural change.

Concretely, given a pretrained model with L linear layers, let $W_l^{\text{PT}} \in \mathbb{R}^{d_{\text{out}}^{(l)} \times d_{\text{in}}^{(l)}}$ denote the weight matrix of the l -th layer. Here, $d_{\text{in}}^{(l)}$ and $d_{\text{out}}^{(l)}$ represent the input and output dimensions of layer l , respectively. We define $\mathbb{W}^{\text{PT}} = \{W_l^{\text{PT}} \mid l \in [1, L]\}$ as the set of weights of the pretrained model. We can perform either full or parameter-efficient finetuning on the base model towards N downstream tasks, obtaining task-specific models $\{\mathbb{W}^{(1)}, \mathbb{W}^{(2)}, \dots, \mathbb{W}^{(N)}\}$.

The **objective** is to combine the finetuned models into a single multitask-capable model \mathbb{W}^{M} that performs well on all of the N tasks on average. In our settings, we consider merging the *weight deltas*, which represent the parameter difference from the base model in matrix form; defined as $\Delta W_l^{(t)} = W_l^{(t)} - W_l^{\text{PT}}$, for each task t and layer l , instead of merging the model weights directly.

3.1 Different finetuned models may not share the same weight parameterizations

Finetuned models typically remain close to the base pretrained model in parameter space—resulting in small *weight deltas* [62]—this might suggest that merging such models, which seemingly share similar weight configurations and semantics, should be straightforward. However, our argument is that *coordinating the weights before merging is essential*. This is because, despite the small magnitude and proximity of the weight deltas, the arrangement of features within them can still diverge across tasks for the following reasons:

Finetuning can lead to change in contextualization. Weights in the hidden layers are contextualized by the adjacent layers, in a way that their feature configurations and orderings have to be in accordance. But as parameter updates from finetuning propagated into the network, it leads to changes in activations, allowing alteration to the contextualization and thus feature arrangement.

The optimization path is non-unique in parameter space. Although, under the infinite width assumption, neural networks follow a deterministic trajectory in *functional space* during training [37], this does not guarantee a unique solution in *parameter space*. In fact, different model parameterizations may lead to functionally equivalent models. These weight symmetries are supported by empirical findings in weight permutation studies [58, 54, 74, 20, 3, 39, 72], which suggests that even under the same pretrained feature space, functionally similar features can be manipulated into different arrangements throughout the course of finetuning.

3.2 Neuron polysemanticity in neural networks

Artificial neurons are often assumed to fire when recognizing a single specific feature it learned. But recent findings demonstrate that these neurons are often polysemantic [57, 56, 19, 67, 53], responding to multiple seemingly unrelated concepts [55]. With a single neuron carrying a composition of features, *weight delta decomposition is required* to enable further interpretation and comparison of their underlying representations [6, 30, 10, 41, 18]. In the rest of this work, we use the term *feature* and *representation* interchangeably.

4 Proposed Method: Decom-Renorm-Merge

4.1 Hypothesis

Building on the above observations, we know that weight delta entries at identical positions do not necessarily encode consistent semantics or functionalities. This invalidates direct entry-wise interference reduction of the weight delta matrices. We make the following hypothesis: weight deltas of differently adapted models *must be decomposed and then coordinated into an identical representation space*, before proper interference reduced merging can be carried out.

4.2 Algorithm

With the hypothesis in mind, we propose **Decom-Renorm-Merge (DRM)**, comprises (1) shared decomposition via SVD, for aligning different weight deltas into a joint representation space, (2) per-task renormalization for stabilizing each individual basis and enabling downstream interference reductions, (3) TIES’ operations applied in the Decompose-renormalized joint space, including pruning, sign election, and disjoint averaging. See Appendix E for analysis on different decompositions.

Concretely, our method consists of the following steps:

1) Joint Decomposition: For each linear layer l , we concatenate the weight deltas $\{\Delta W_l^{(t)}\}_{t=1}^N$ horizontally across N tasks, and apply SVD,

$$\Delta W_l^{\text{stack}} = [\Delta W_l^{(1)} \ \Delta W_l^{(2)} \ \dots \ \Delta W_l^{(N)}] \quad (1)$$

$$= U \Sigma V^T \quad (2)$$

where $U \in \mathbb{R}^{d_{\text{out}}^{(l)} \times d_{\text{out}}^{(l)}}$ is the shared left singular vector matrix (representing joint output feature basis), $\Sigma \in \mathbb{R}^{d_{\text{out}}^{(l)} \times N d_{\text{in}}^{(l)}}$ contains singular values (capturing each basis direction’s shared importance across task), and $V^T \in \mathbb{R}^{N d_{\text{in}}^{(l)} \times N d_{\text{in}}^{(l)}}$ is the right singular vector matrix.

2) Partition: We partition the full right singular vector matrix V^T into task-specific blocks,

$$\Delta W_l^{\text{stack}} = U \Sigma [V_1^T \ V_2^T \ \dots \ V_N^T] \quad (3)$$

where each $V_t^T \in \mathbb{R}^{N d_{\text{in}}^{(l)} \times d_{\text{in}}^{(l)}}$ corresponds to task t . Note that each task’s original weight delta can be reconstructed by,

$$\Delta W_l^{(t)} = U \Sigma V_t^T \quad (4)$$

3) Renormalization. The rows of V_t^T are generally not of unit lengths due to the partitioning. For each row $v_{t,i}$, we renormalize the vector,

$$\tilde{v}_{t,i} = \frac{v_{t,i}}{\|v_{t,i}\|_2} \quad (5)$$

Collectively, this yields a renormalized matrix \tilde{V}_t^T . The original row norms are redistributed into the singular values,

$$\Sigma_t = \Sigma \hat{V}_t \quad (6)$$

where \hat{V}_t is a diagonal matrix with entries $\|v_{t,i}\|_2$ on the diagonal, and Σ_t is now the singular value matrix of the renormalized task t specifically.

4) Pruning: For each task t , we keep only the top- $k\%$ largest-magnitude entries in \tilde{V}_t^T , and zero out the others. It is vital that this step be done after renormalization to ensure stability, pruning on unnormalized magnitudes could distort the basis vectors. We set the default to top-20%

5) Sign Election: To resolve inter-task sign conflicts, we compute a sign mask, $S = \text{sgn}(\sum_{t=1}^N \Sigma_t \tilde{V}_t^T)$, selecting a magnitude dominant sign for each position. Then, we zero out entries with signs opposite to the elected mask. This procedure is done in scale-variant fashion by multiplying the Σ_t in.

6) Disjoint Averaging: We compute the disjoint average of the processed $\Sigma_t \tilde{V}_t^T$, considering only non-zero entries,

$$(\Sigma \tilde{V}^T)^M = \Gamma \odot \sum_{t=1}^N \lambda_t \Sigma_t \tilde{V}_t^T \quad (7)$$

Here, λ_t is a task-specific scalar weighting coefficient, with default $\lambda = 1.0$ for all tasks. Γ is an entry-wise averaging reciprocal mask that ensures averaging procedure is performed only over non-zero entries. We define $\Gamma \in \mathbb{R}^{m \times n}$ with entry at row i , column j as the following reciprocal:

$$\Gamma_{i,j} = \frac{1}{\sum_{t=1}^N \mathbb{1}(\Delta W_{t,i,j} \neq 0)} \quad (8)$$

Table 1: Merging results of vision and language models, with and with no validation set available. We report all results in classification accuracy. **Bold** represents the best score, and underline represents the second best.

Methods	Validation	Vision Models		Language Models		
		ViT-B/32	ViT-L/14	DeB-Base	T5-Base	T5-Large
Finetune		90.8	94.3	83.4	85.1	89.3
Simple Averaging	×	66.1	79.6	<u>57.6</u>	63.3	73.2
Task Arithmetic	×	60.6	83.4	<u>55.4</u>	76.4	80.1
TIES Merging	×	72.5	86.1	48.7	71.8	72.3
Dare-TIES	×	71.1	85.9	47.3	72.3	72.3
DRM-H	×	77.5	88.0	66.9	<u>73.6</u>	<u>74.5</u>
DRM-V	×	<u>72.8</u>	<u>86.3</u>	54.1	72.8	73.3
Task Arithmetic	✓	70.3	84.6	58.1	76.4	80.1
TIES Merging	✓	74.3	<u>86.9</u>	57.2	73.7	<u>79.5</u>
Dare-TIES	✓	74.4	86.8	57.8	74.6	<u>79.5</u>
DRM-H	✓	78.3	89.3	67.9	74.4	75.1
DRM-V	✓	<u>74.6</u>	86.4	<u>61.1</u>	<u>75.1</u>	77.4

7) **Reconstruction:** We transform the merged representation back into the original parameter space,

$$\Delta W_l^M = U(\Sigma \tilde{V}^T)^M \quad (9)$$

and recover the full merged weight,

$$W_l^M = W_l^{\text{PT}} + \Delta W_l^M \quad (10)$$

For other parameters such as bias terms and affine weights, weighted averaging is applied using the weights λ_t . Ultimately, the same algorithm can also be carried out vertically through U_t , as for aligning into joint row basis instead. We denote the horizontal stacking version of our algorithm *DRM-H*, and the vertical counterpart *DRM-V*. We demonstrate their differences in the subsequent sections.

5 Experiments

In this section, we test our proposed merging method experimentally. We directly evaluate the merging performance on different model architectures, tasks, and finetuning approaches. We then test the method’s sensitivity and ablate the significance of our algorithmic component.

5.1 Baselines

For comparison, we replicate and evaluate our methods against the following four methods:

1. **Simple Averaging** compute the average of every model’s weights, $W_l^M = \frac{1}{N} \sum_{t=1}^N W_l^{(t)}$.
2. **Task Arithmetic** [35] performs a weighted averaging on the weight deltas, $W_l^M = W_l^{\text{PT}} + \sum_{t=1}^N \lambda_t \Delta W_l^{(t)}$. We follow [83] and set the default to a shared $\lambda = 0.4$.
3. **TIES Merging** [83] first prunes the low magnitude weights. Then, reduces sign conflicts by electing a dominant magnitude sign for each parameter location, and keep only parameters with the same sign as the elected. Afterwards, only the kept parameters are averaged. As in the original paper, we set the default to retaining top-20%, and a shared λ of 1.0.
4. **DARE-TIES** [85] extends TIES Merging, by replacing magnitude pruning with a random drop of rate p and a rescale with $\frac{1}{1-p}$. We again set the default to retaining top-20%, and a shared λ of 1.0.

5.2 Results

Merging Vision Models. We start with merging of image classification models, following [35]. We use ViT-B/32 and ViT-L/14 [15] visual encoders of CLIP [61], finetune them to eight datasets

Table 2: Merging results of low-rank fine-tuned Llama 3.1-8B’s across five different tasks with and without validation set scenarios. We report all results in classification accuracy. **Bold** represents the best score, and underline represents the second best. Average performance of finetuned Llama 3.1-8B across every task is 90.5.

Models	Validation	Methods					
		Averaging	Task Arithmetic	TIES	Dare-TIES	DRM-H	DRM-V
Llama 3.1-8B	×	61.5	45.9	67.1	67.6	69.5	<u>69.1</u>
	✓		66.4	69.4	68.8	<u>73.3</u>	74.3

separately: Cars [44], DTD [13], EuroSAT [28], GTSRB [71], MNIST [45], RESISC45 [11], SUN397 [82], and SVHN [52]. We report the results in Table 1. Using DRM-H to merge fully finetuned ViT-B/32 and ViT-L/14 yields improvements of 5.0% and 1.9% respectively over the strongest baselines. Tuning on validation sets yields improvements of 3.9% and 2.4% over strongest baselines. Remarkably, DRM-H without hyperparameter tuning outperforms baselines with tuning. For performance breakdown of each task, refer to Appendix H.6.

Merging Language Models. For merging of language models, we adopt a similar setting to [38] and experiment on encoder-only models: DeBERTa-Large-V3 [27], and encoder-decoder based: T5-Base, and T5-Large [63]. Following [83] closely, we finetune the models to six NLU tasks: question answering (QASC [40], WikiQA [84], and QuaRTz [73]), paraphrase identification (PAWS [86]), story completion (Story Cloze [51]), and coreference resolution (Winogrande [66]). Table 1 shows that DRM-H improves the performance by 9.3% in merging DeBERTa-Base-V3. Tuning on validation set improves the margin to 9.8% over the strongest baseline.

Merging LoRA-adapted Large Language Models. For merging of large language models, we adapt Llama3.1-8B [76] to five GLUE tasks individually: MNLI [80], QNLI [78], RTE [78], COLA [79], and SST2 [70] For this setup, we perform low-rank adaptation ($r = 16$) instead of full finetuning as done previously. Table 2 shows that without validation data (no hyperparameter tuning), DRM-H outperforms other competitors by more than 1.9%. In the presence of hyperparameter tuning, DRM-V outperforms the strongest baseline by a margin of 3.9%. Notice that, unlike in the previous winning scenarios, where DRM-V is usually subpar or relatively close to DRM-H. Reversed here, DRM-V with hyperparameter tuning surpasses DRM-H by a margin of 1.0%. We provide analysis on this phenomenon in Appendix G.

5.3 Additional Results And Analysis

Merging Different Number of Models. In this study, we experiment with varying the number of tasks being merged as done in [35, 83]. We compare our DRM-H with Simple Averaging, TIES Merging, and DARE-TIES on two models: ViT-B/32 and T5-Base, Each point represents result on a single subset of the tasks, and the solid line represents the average performance for each subset size. Note that we only sample at most 10 distinct combinations for each subset size. From Figure 2, we see that at 2 or 3 tasks, performance of most merging techniques stay close together. But as the number of tasks grows, DRM-H maintains highest merging performances, suggesting that DRM-H scales better to a large number of tasks.

Table 3: Comparison of merging results with and without renormalization on DRM-H. We observe that renormalization improves performance of the merged models by a large margin, most prominently in DeBERTa-Base with a 8.8% difference.

	Renorm	ViT-B/32	T5-B	DeB-B	Llama-8B
✓		77.5	73.6	66.9	69.5
×		73.5	68.6	58.1	62.7

Ablation of Renormalization. This experiment investigates the performance impact of renormalization in our merging algorithm. We ablate performing merging, with and without applying renormalization to the joint representation space. Table 3 demonstrates that renormalization provides enormous gain to the merging performance. The improvement ranges from 4.0% in ViT-B/32, 5.0% in T5-Base, 8.8% in DeBERTa-Base, and 6.8% in Llama3.1-8B.

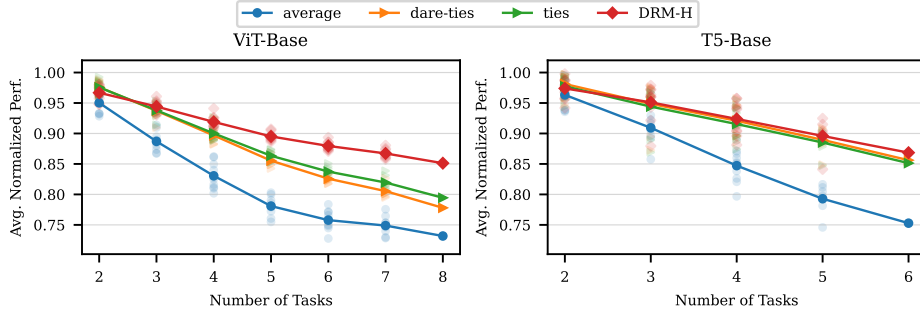


Figure 2: Results obtained when merging different number of tasks. DRM-H maintains better performance as the number of merged tasks increased.

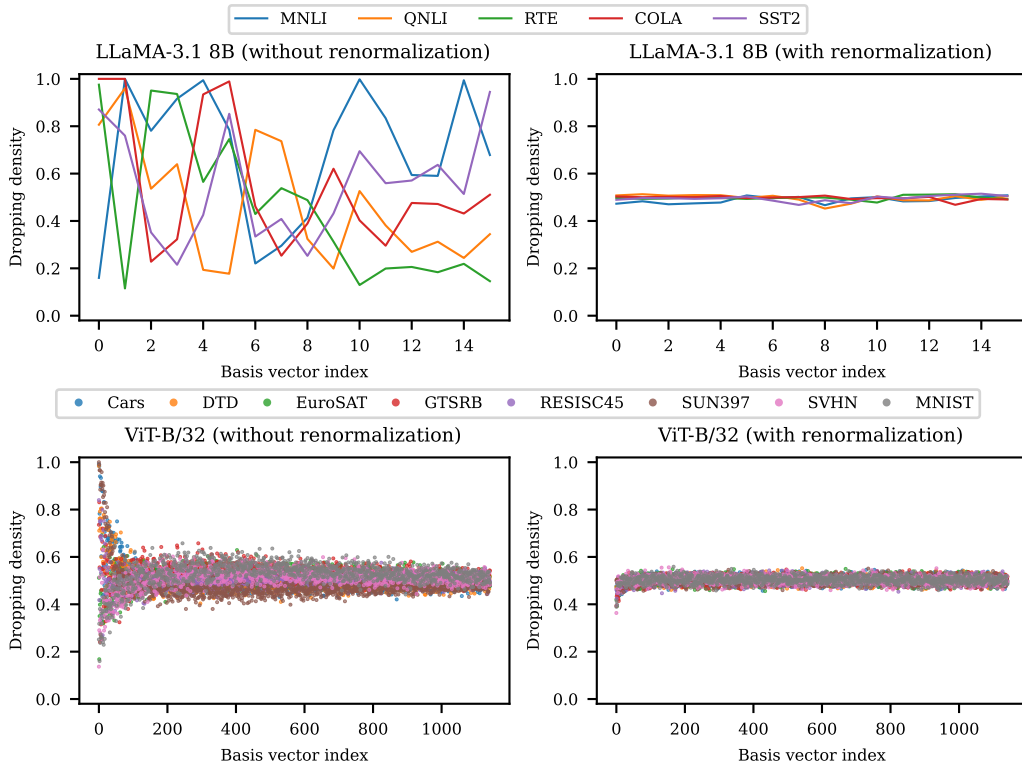


Figure 3: Percentages of entries being dropped from each row basis vector $v_{t,i}$ during the pruning of entire matrices: **(Top)** the middle LoRA layer (16th) of Llama-3.1 8B, with and without renormalization. **(Bottom)** weight deltas of the middle layer (6th) of ViT-B/32, with and without renormalization. Here, we prune 50% of each matrix. The dropped percentages fluctuate severely without renormalization, with some vectors almost entirely zeroed out.

6 Understanding the Decompose-Renormalized Joint Space

Seeing the empirical verification of the DRM, we hope to understand more about our method, particularly the intrinsic nature of the Decompose-renormalized joint space used for the merging.

We perform a series of studies to answer the following questions: 1) Why is it crucial that magnitude pruning be done on renormalized singular vector matrices? Shouldn't pruning on unrenormalized basis vector matrices be even better? Since they better capture the real scale of each basis entry. 2) How does reducing interference on the Decompose-renormalized space reflect interference on the original parameter space? Does reducing interference in one space directly influence the other?

6.1 Why is it Crucial that Weight Pruning be Done on Renormalized Singular Vector Matrices?

After partitioning the right singular vector matrix V^T from the concatenated SVD, the row basis vectors lose the orthonormal property. We renormalize each row to unit norm² before applying interference reduction techniques. As shown in Section 5.3, renormalization is central to DRM. We present the investigation of effect of renormalization on the pruning behavior in Figure 3. It displays the percentages of entries being dropped from each basis vector. We see that without renormalization, the dropping densities oscillate severely, with some vectors have almost all of their entries zeroed out. Removing top principle components like this would quickly deteriorate downstream performance. By adding in renormalization, the dropping densities are stabilized evenly across all vectors, bounded to around the configured prune rate of 50%, no single vector will be wholly pruned.

6.2 How Does Pruning on Decompose-renormalized Space Reflect Interference in Original Parameter Space?

In TIES Merging [83], the authors demonstrate that two major interference sources are redundant parameter values, and sign disagreements at corresponding positions in the weight delta matrices. They hypothesized that mitigating these interferences would enhance merging performance.

However, our analysis in Table 4 reveals that although pruning in the Decompose-renormalized space effectively improves merging performance, it does not result in higher sign agreement when projected back to the original parameter space. Specifically, we first project the weight deltas into the Decompose-renormalized space, apply pruning to the basis entries. We then transform the results back to the original space and measure sign agreement, but we found no improvement.

Nevertheless, DRM still achieves mostly superior merging performance compared to methods reducing interference directly in the original parameter space. This suggests that interference reduction techniques lead to the most effective merging when applied in the Decompose-renormalized space, rather than directly on individual parameter entries. See Appendix F for more detailed results and comparison with no pruning applied.

Table 4: Average sign agreement after pruning different spaces. We compare between pruning in the original parameter space (labeled *Original Weight*), versus pruning in the joint singular space. For the latter, sign agreement is measured in both the joint singular space (labeled *DS*), and after projecting back to the original space (labeled *OS*). Results demonstrate that reducing interference on the joint space does not correspond to higher sign agreement in the original parameter space. Note that the minimum sign agreement is 50%, when there are an equal number of positive and negative entries.

	Space	ViT-B/32	Llama-8B
Original Weight	-	86.6	91.0
Horizontal	DS	84.4	89.7
	OS	71.0	70.6
Vertical	DS	86.1	89.9
	OS	69.5	70.2

7 Conclusion

In this work, we addressed a fundamental limitation in existing interference reduction-based model merging techniques that assume consistent feature composition and arrangement across independently finetuned models. To overcome the challenge, we introduced Decom-Renorm-Merge (DRM), an effective approach that combines singular value decomposition and renormalization for establishing a shared representation space, enabling entry-wise interference reduction techniques and merging to be properly applied within. Our experiments demonstrated that DRM outperformed several state-of-the-art merging techniques across diverse architectures and task modalities. Further analysis provided insights into the crucial role of joint space renormalization, and the necessity of performing interference reduction within the Decompose-renormalized space rather than directly on the parameters. These results further our understanding of effective model merging and provide a means for more efficient knowledge fusion in neural networks.

²Unlike the unit length property, orthogonality of the split matrices, is not easily reattainable. We observe that enforcing orthogonality through Gram-Schmidt process harshly degrades the performance.

8 Acknowledgements

We are grateful to Artit Suwanbandit and Patawee Prakrankamanant for inspiration and insightful discussions early into this work.

References

- [1] Aakanksha, Arash Ahmadian, Seraphina Goldfarb-Tarrant, Beyza Ermis, Marzieh Fadaee, and Sara Hooker. Mix data or merge models? Optimizing for performance and safety in multilingual contexts. In *Neurips Safe Generative AI Workshop 2024*, 2024. URL <https://openreview.net/forum?id=L1Hxp8ktiT>.
- [2] Joshua Ainslie, James Lee-Thorp, Michiel de Jong, Yury Zemlyanskiy, Federico Lebron, and Sumit Sanghai. Gqa: Training generalized multi-query transformer models from multi-head checkpoints. In *Proceedings of the 2023 Conference on Empirical Methods in Natural Language Processing*, pages 4895–4901, 2023.
- [3] Samuel Ainsworth, Jonathan Hayase, and Siddhartha Srinivasa. Git Re-Basin: Merging models modulo permutation symmetries. In *The Eleventh International Conference on Learning Representations*, 2023. URL <https://openreview.net/forum?id=CQsmMYm1P5T>.
- [4] Sanjeev Arora, Yuanzhi Li, Yingyu Liang, Tengyu Ma, and Andrej Risteski. Linear algebraic structure of word senses, with applications to polysemy. *Transactions of the Association for Computational Linguistics*, 6:483–495, 2018. doi: 10.1162/tac1_a_00034. URL <https://aclanthology.org/Q18-1034/>.
- [5] Devansh Arpit, Huan Wang, Yingbo Zhou, and Caiming Xiong. Ensemble of averages: Improving model selection and boosting performance in domain generalization. In *Advances in Neural Information Processing Systems*, 2022. URL <https://openreview.net/forum?id=peZSbfNnBp4>.
- [6] Yoshua Bengio, Aaron Courville, and Pascal Vincent. Representation learning: a review and new perspectives. *IEEE transactions on pattern analysis and machine intelligence*, 35(8):1798–1828, August 2013. ISSN 0162-8828. doi: 10.1109/tpami.2013.50. URL <http://www.cs.princeton.edu/courses/archive/spring13/cos598C/RepresentationLearning-AReviewandNewPerspectives.pdf>.
- [7] Tom Brown, Benjamin Mann, Nick Ryder, Melanie Subbiah, Jared D Kaplan, Prafulla Dhariwal, Arvind Neelakantan, Pranav Shyam, Girish Sastry, Amanda Askell, et al. Language models are few-shot learners. *Advances in neural information processing systems*, 33:1877–1901, 2020.
- [8] Rich Caruana. *Multitask learning*, page 95–133. Kluwer Academic Publishers, USA, 1998. ISBN 0792380479.
- [9] Junbum Cha, Sanghyuk Chun, Kyungjae Lee, Han-Cheol Cho, Seunghyun Park, Yunsung Lee, and Sungrae Park. SWAD: Domain generalization by seeking flat minima. In *Advances in Neural Information Processing Systems*, volume 34, pages 22405–22418. Curran Associates, Inc., 2021. URL https://proceedings.neurips.cc/paper_files/paper/2021/file/bcb41ccdc4363c6848a1d760f26c28a0-Paper.pdf.
- [10] Xi Chen, Yan Duan, Rein Houthoofd, John Schulman, Ilya Sutskever, and Pieter Abbeel. InfoGAN: Interpretable representation learning by information maximizing generative adversarial nets. In *Advances in Neural Information Processing Systems*, volume 29. Curran Associates, Inc., 2016. URL https://proceedings.neurips.cc/paper_files/paper/2016/file/7c9d0b1f96aebd7b5eca8c3edaa19ebb-Paper.pdf.
- [11] Gong Cheng, Junwei Han, and Xiaoqiang Lu. Remote sensing image scene classification: Benchmark and state of the art. *Proceedings of the IEEE*, 105(10):1865–1883, 2017. doi: 10.1109/JPROC.2017.2675998.
- [12] Leshem Choshen, Elad Venezian, Noam Slonim, and Yoav Katz. Fusing finetuned models for better pretraining, 2022. URL <https://arxiv.org/abs/2204.03044>.

- [13] Mircea Cimpoi, Subhransu Maji, Iasonas Kokkinos, Sammy Mohamed, and Andrea Vedaldi. Describing textures in the wild. In *Proceedings of the IEEE Conference on Computer Vision and Pattern Recognition (CVPR)*, June 2014.
- [14] Tri Dao. Flashattention-2: Faster attention with better parallelism and work partitioning. In *The Twelfth International Conference on Learning Representations*, 2024. URL <https://openreview.net/forum?id=mZn2Xyh9Ec>.
- [15] Alexey Dosovitskiy, Lucas Beyer, Alexander Kolesnikov, Dirk Weissenborn, Xiaohua Zhai, Thomas Unterthiner, Mostafa Dehghani, Matthias Minderer, Georg Heigold, Sylvain Gelly, Jakob Uszkoreit, and Neil Houlsby. An image is worth 16x16 words: Transformers for image recognition at scale. In *International Conference on Learning Representations*, 2021. URL <https://openreview.net/forum?id=YicbFdNTTy>.
- [16] Felix Draxler, Kambis Veschgini, Manfred Salmhofer, and Fred Hamprecht. Essentially no barriers in neural network energy landscape. In *Proceedings of the 35th International Conference on Machine Learning*, volume 80 of *Proceedings of Machine Learning Research*, pages 1309–1318. PMLR, 10–15 Jul 2018. URL <https://proceedings.mlr.press/v80/draxler18a.html>.
- [17] Carl Eckart and Gale Young. The approximation of one matrix by another of lower rank. *Psychometrika*, 1(3):211–218, 1936.
- [18] Nelson Elhage, Tristan Hume, Catherine Olsson, Neel Nanda, Tom Henighan, Scott Johnston, Sheer ElShowk, Nicholas Joseph, Nova DasSarma, Ben Mann, Danny Hernandez, Amanda Askell, Kamal Ndousse, Andy Jones, Dawn Drain, Anna Chen, Yuntao Bai, Deep Ganguli, Liane Lovitt, Zac Hatfield-Dodds, Jackson Kernion, Tom Conerly, Shauna Kravec, Stanislav Fort, Saurav Kadavath, Josh Jacobson, Eli Tran-Johnson, Jared Kaplan, Jack Clark, Tom Brown, Sam McCandlish, Dario Amodei, and Christopher Olah. Softmax linear units. *Transformer Circuits Thread*, 2022. <https://transformer-circuits.pub/2022/solu/index.html>.
- [19] Nelson Elhage, Tristan Hume, Catherine Olsson, Nicholas Schiefer, Tom Henighan, Shauna Kravec, Zac Hatfield-Dodds, Robert Lasenby, Dawn Drain, Carol Chen, Roger Grosse, Sam McCandlish, Jared Kaplan, Dario Amodei, Martin Wattenberg, and Christopher Olah. Toy models of superposition. *Transformer Circuits Thread*, 2022. https://transformer-circuits.pub/2022/toy_model/index.html.
- [20] Rahim Entezari, Hanie Sedghi, Olga Saukh, and Behnam Neyshabur. The role of permutation invariance in linear mode connectivity of neural networks. In *International Conference on Learning Representations*, 2022. URL <https://openreview.net/forum?id=dNigytemkL>.
- [21] Jonathan Frankle, Gintare Karolina Dziugaite, Daniel Roy, and Michael Carbin. Linear mode connectivity and the lottery ticket hypothesis. In *Proceedings of the 37th International Conference on Machine Learning*, volume 119 of *Proceedings of Machine Learning Research*, pages 3259–3269. PMLR, 13–18 Jul 2020. URL <https://proceedings.mlr.press/v119/frankle20a.html>.
- [22] C. Daniel Freeman and Joan Bruna. Topology and geometry of half-rectified network optimization. In *International Conference on Learning Representations*, 2017. URL <https://openreview.net/forum?id=Bk0FWVcgx>.
- [23] Timur Garipov, Pavel Izmailov, Dmitrii Podoprikin, Dmitry P Vetrov, and Andrew G Wilson. Loss surfaces, mode connectivity, and fast ensembling of dnns. In *Advances in Neural Information Processing Systems*, volume 31. Curran Associates, Inc., 2018. URL https://proceedings.neurips.cc/paper_files/paper/2018/file/be3087e74e9100d4bc4c6268cdbc8456-Paper.pdf.
- [24] Aaron Grattafiori, Abhimanyu Dubey, Abhinav Jauhri, Abhinav Pandey, Abhishek Kadian, Ahmad Al-Dahle, Aiesha Letman, Akhil Mathur, Alan Schelten, Alex Vaughan, et al. The Llama 3 herd of models. *arXiv preprint arXiv:2407.21783*, 2024.
- [25] Vipul Gupta, Santiago Akle Serrano, and Dennis DeCoste. Stochastic weight averaging in parallel: Large-batch training that generalizes well. In *International Conference on Learning Representations*, 2020. URL <https://openreview.net/forum?id=rygFWAEfWS>.

- [26] Pengcheng He, Jianfeng Gao, and Weizhu Chen. DeBERTaV3: Improving DeBERTa using ELECTRA-style pre-training with gradient-disentangled embedding sharing. *CoRR*, abs/2111.09543, 2021. URL <https://arxiv.org/abs/2111.09543>.
- [27] Pengcheng He, Xiaodong Liu, Jianfeng Gao, and Weizhu Chen. DeBERTa: Decoding-enhanced BERT with disentangled attention. In *International Conference on Learning Representations*, 2021. URL <https://openreview.net/forum?id=XPZiaotutsD>.
- [28] Patrick Helber, Benjamin Bischke, Andreas Dengel, and Damian Borth. Eurosat: A novel dataset and deep learning benchmark for land use and land cover classification. *IEEE Journal of Selected Topics in Applied Earth Observations and Remote Sensing*, 2019.
- [29] Tom Henighan, Shan Carter, Tristan Hume, Nelson Elhage, Robert Lasenby, Stanislaw Fort, Nicholas Schiefer, and Christopher Olah. Superposition, memorization, and double descent. *Transformer Circuits Thread*, 6:24, 2023.
- [30] Irina Higgins, Loic Matthey, Arka Pal, Christopher Burgess, Xavier Glorot, Matthew Botvinick, Shakir Mohamed, and Alexander Lerchner. beta-VAE: Learning basic visual concepts with a constrained variational framework. In *International Conference on Learning Representations*, 2017. URL <https://openreview.net/forum?id=Sy2fzU9g1>.
- [31] Christopher J Hillar and Lek-Heng Lim. Most tensor problems are np-hard. *Journal of the ACM (JACM)*, 60(6):1–39, 2013.
- [32] Pin-Lun Hsu, Yun Dai, Vignesh Kothapalli, Qingquan Song, Shao Tang, Siyu Zhu, Steven Shimizu, Shivam Sahni, Haowen Ning, and Yanning Chen. Liger kernel: Efficient triton kernels for llm training. *arXiv preprint arXiv:2410.10989*, 2024.
- [33] Edward J Hu, yelong shen, Phillip Wallis, Zeyuan Allen-Zhu, Yuanzhi Li, Shean Wang, Lu Wang, and Weizhu Chen. LoRA: Low-rank adaptation of large language models. In *International Conference on Learning Representations*, 2022. URL <https://openreview.net/forum?id=nZeVKeeFYf9>.
- [34] Gabriel Ilharco, Mitchell Wortsman, Ross Wightman, Cade Gordon, Nicholas Carlini, Rohan Taori, Achal Dave, Vaishaal Shankar, Hongseok Namkoong, John Miller, Hannaneh Hajishirzi, Ali Farhadi, and Ludwig Schmidt. OpenCLIP. Zenodo, July 2021. doi: 10.5281/zenodo.5143773. URL <https://doi.org/10.5281/zenodo.5143773>.
- [35] Gabriel Ilharco, Marco Tulio Ribeiro, Mitchell Wortsman, Ludwig Schmidt, Hannaneh Hajishirzi, and Ali Farhadi. Editing models with task arithmetic. In *The Eleventh International Conference on Learning Representations*, 2023. URL <https://openreview.net/forum?id=6t0Kwf8-jrj>.
- [36] Pavel Izmailov, Dmitrii Podoprikin, Timur Garipov, Dmitry Vetrov, and Andrew Gordon Wilson. Averaging weights leads to wider optima and better generalization, 2019. URL <https://arxiv.org/abs/1803.05407>.
- [37] Arthur Jacot, Franck Gabriel, and Clement Hongler. Neural tangent kernel: Convergence and generalization in neural networks. In *Advances in Neural Information Processing Systems*, volume 31. Curran Associates, Inc., 2018. URL https://proceedings.neurips.cc/paper_files/paper/2018/file/5a4be1fa34e62bb8a6ec6b91d2462f5a-Paper.pdf.
- [38] Xisen Jin, Xiang Ren, Daniel Preotiuc-Pietro, and Pengxiang Cheng. Dataless knowledge fusion by merging weights of language models. In *The Eleventh International Conference on Learning Representations*, 2023. URL <https://openreview.net/forum?id=FCnohuR6AnM>.
- [39] Keller Jordan, Hanie Sedghi, Olga Saukh, Rahim Entezari, and Behnam Neyshabur. REPAIR: RENormalizing permuted activations for interpolation repair. In *The Eleventh International Conference on Learning Representations*, 2023. URL <https://openreview.net/forum?id=gU5sJ6ZggcX>.
- [40] Tushar Khot, Peter Clark, Michal Guerquin, Peter Jansen, and Ashish Sabharwal. QASC: A dataset for question answering via sentence composition. *arXiv:1910.11473v2*, 2020.

- [41] Hyunjik Kim and Andriy Mnih. Disentangling by factorising. In *Proceedings of the 35th International Conference on Machine Learning*, volume 80 of *Proceedings of Machine Learning Research*, pages 2649–2658. PMLR, 10–15 Jul 2018. URL <https://proceedings.mlr.press/v80/kim18b.html>.
- [42] Tamara G Kolda and Brett W Bader. Tensor decompositions and applications. *SIAM review*, 51(3):455–500, 2009.
- [43] Jean Kossaifi, Yannis Panagakis, Anima Anandkumar, and Maja Pantic. Tensorly: Tensor learning in python. *Journal of Machine Learning Research*, 20(26):1–6, 2019.
- [44] Jonathan Krause, Michael Stark, Jia Deng, and Li Fei-Fei. 3D object representations for fine-grained categorization. In *2013 IEEE International Conference on Computer Vision Workshops*, pages 554–561, 2013. doi: 10.1109/ICCVW.2013.77.
- [45] Y. Lecun, L. Bottou, Y. Bengio, and P. Haffner. Gradient-based learning applied to document recognition. *Proceedings of the IEEE*, 86(11):2278–2324, 1998. doi: 10.1109/5.726791.
- [46] Hector Levesque, Ernest Davis, and Leora Morgenstern. The winograd schema challenge. In *Thirteenth International Conference on the Principles of Knowledge Representation and Reasoning*. Citeseer, 2012.
- [47] Aixin Liu, Bei Feng, Bing Xue, Bingxuan Wang, Bochao Wu, Chengda Lu, Chenggang Zhao, Chengqi Deng, Chenyu Zhang, Chong Ruan, et al. Deepseek-v3 technical report. *arXiv preprint arXiv:2412.19437*, 2024.
- [48] Chang Liu, Chenfei Lou, Runzhong Wang, Alan Yuhan Xi, Li Shen, and Junchi Yan. Deep neural network fusion via graph matching with applications to model ensemble and federated learning. In *Proceedings of the 39th International Conference on Machine Learning*, volume 162 of *Proceedings of Machine Learning Research*, pages 13857–13869. PMLR, 17–23 Jul 2022. URL <https://proceedings.mlr.press/v162/liu22k.html>.
- [49] Ilya Loshchilov and Frank Hutter. Decoupled weight decay regularization. In *International Conference on Learning Representations*, 2019. URL <https://openreview.net/forum?id=Bkg6RiCqY7>.
- [50] Michael Matena and Colin Raffel. Merging models with fisher-weighted averaging, 2022. URL <https://arxiv.org/abs/2111.09832>.
- [51] Nasrin Mostafazadeh, Michael Roth, Annie Louis, Nathanael Chambers, and James Allen. Lsdsem 2017 shared task: The story cloze test. In *Proceedings of the 2nd Workshop on Linking Models of Lexical, Sentential and Discourse-level Semantics*, pages 46–51, 2017.
- [52] Yuval Netzer, Tao Wang, Adam Coates, Alessandro Bissacco, Bo Wu, and Andrew Y. Ng. Reading digits in natural images with unsupervised feature learning. In *NIPS Workshop on Deep Learning and Unsupervised Feature Learning 2011*, 2011. URL http://ufldl.stanford.edu/housenumbers/nips2011_housenumbers.pdf.
- [53] Anh Mai Nguyen, Jason Yosinski, and Jeff Clune. Multifaceted feature visualization: Uncovering the different types of features learned by each neuron in deep neural networks. *CoRR*, abs/1602.03616, 2016. URL <http://arxiv.org/abs/1602.03616>.
- [54] Thao Nguyen, Maithra Raghu, and Simon Kornblith. Do wide and deep networks learn the same things? Uncovering how neural network representations vary with width and depth. In *International Conference on Learning Representations*, 2021. URL <https://openreview.net/forum?id=KJNcAkY8tY4>.
- [55] Chris Olah, Alexander Mordvintsev, and Ludwig Schubert. Feature visualization. *Distill*, 2017. doi: 10.23915/distill.00007. <https://distill.pub/2017/feature-visualization>.
- [56] Chris Olah, Nick Cammarata, Ludwig Schubert, Gabriel Goh, Michael Petrov, and Shan Carter. An overview of early vision in InceptionV1. *Distill*, 2020. doi: 10.23915/distill.00024.002. <https://distill.pub/2020/circuits/early-vision>.

- [57] Chris Olah, Nick Cammarata, Ludwig Schubert, Gabriel Goh, Michael Petrov, and Shan Carter. Zoom in: An introduction to circuits. *Distill*, 2020. doi: 10.23915/distill.00024.001. <https://distill.pub/2020/circuits/zoom-in>.
- [58] Chris Olah, Nick Cammarata, Chelsea Voss, Ludwig Schubert, and Gabriel Goh. Naturally occurring equivariance in neural networks. *Distill*, 2020. doi: 10.23915/distill.00024.004. <https://distill.pub/2020/circuits/equivariance>.
- [59] Guillermo Ortiz-Jimenez, Alessandro Favero, and Pascal Frossard. Task arithmetic in the tangent space: Improved editing of pre-trained models. In *Thirty-seventh Conference on Neural Information Processing Systems*, 2023. URL <https://openreview.net/forum?id=OA9f2jZDGW>.
- [60] Fidel A. Guerrero Peña, Heitor Rapela Medeiros, Thomas Dubail, Masih Aminbeidokhti, Eric Granger, and Marco Pedersoli. Re-basin via implicit Sinkhorn differentiation, 2022. URL <https://arxiv.org/abs/2212.12042>.
- [61] Alec Radford, Jong Wook Kim, Chris Hallacy, Aditya Ramesh, Gabriel Goh, Sandhini Agarwal, Girish Sastry, Amanda Askell, Pamela Mishkin, Jack Clark, Gretchen Krueger, and Ilya Sutskever. Learning transferable visual models from natural language supervision. In *Proceedings of the 38th International Conference on Machine Learning*, volume 139 of *Proceedings of Machine Learning Research*, pages 8748–8763. PMLR, 18–24 Jul 2021. URL <https://proceedings.mlr.press/v139/radford21a.html>.
- [62] Evani Radiya-Dixit and Xin Wang. How fine can fine-tuning be? Learning efficient language models. In *Proceedings of the Twenty Third International Conference on Artificial Intelligence and Statistics*, volume 108 of *Proceedings of Machine Learning Research*, pages 2435–2443. PMLR, 26–28 Aug 2020. URL <https://proceedings.mlr.press/v108/radiya-dixit20a.html>.
- [63] Colin Raffel, Noam Shazeer, Adam Roberts, Katherine Lee, Sharan Narang, Michael Matena, Yanqi Zhou, Wei Li, and Peter J. Liu. Exploring the limits of transfer learning with a unified text-to-text transformer. *Journal of Machine Learning Research*, 21(140):1–67, 2020. URL <http://jmlr.org/papers/v21/20-074.html>.
- [64] Alexandre Rame, Matthieu Kirchmeyer, Thibaud Rahier, Alain Rakotomamonjy, patrick gallinari, and Matthieu Cord. Diverse weight averaging for out-of-distribution generalization. In *Advances in Neural Information Processing Systems*, 2022. URL https://openreview.net/forum?id=tq_J_MqB3UB.
- [65] Alexandre Rame, Kartik Ahuja, Jianyu Zhang, Matthieu Cord, Leon Bottou, and David Lopez-Paz. Model Ratatouille: recycling diverse models for out-of-distribution generalization. In *Proceedings of the 40th International Conference on Machine Learning*, volume 202 of *Proceedings of Machine Learning Research*, pages 28656–28679. PMLR, 23–29 Jul 2023. URL <https://proceedings.mlr.press/v202/rame23a.html>.
- [66] Keisuke Sakaguchi, Ronan Le Bras, Chandra Bhagavatula, and Yejin Choi. WinoGrande: an adversarial winograd schema challenge at scale. *Commun. ACM*, 64(9):99–106, August 2021. ISSN 0001-0782. doi: 10.1145/3474381. URL <https://doi.org/10.1145/3474381>.
- [67] Adam Scherlis, Kshitij Sachan, Adam S. Jermyn, Joe Benton, and Buck Shlegeris. Polysemanticity and capacity in neural networks. *CoRR*, abs/2210.01892, 2022. URL <https://doi.org/10.48550/arXiv.2210.01892>.
- [68] Maksym Shamrai. Perturbation analysis of singular values in concatenated matrices. *arXiv preprint arXiv:2505.01427*, 2025.
- [69] Sidak Pal Singh and Martin Jaggi. Model fusion via optimal transport. In *Advances in Neural Information Processing Systems*, volume 33, pages 22045–22055. Curran Associates, Inc., 2020. URL https://proceedings.neurips.cc/paper_files/paper/2020/file/fb2697869f56484404c8ceee2985b01d-Paper.pdf.

- [70] Richard Socher, Alex Perelygin, Jean Wu, Jason Chuang, Christopher D. Manning, Andrew Ng, and Christopher Potts. Recursive deep models for semantic compositionality over a sentiment treebank. In *Proceedings of the 2013 Conference on Empirical Methods in Natural Language Processing*, pages 1631–1642, Seattle, Washington, USA, October 2013. Association for Computational Linguistics. URL <https://aclanthology.org/D13-1170/>.
- [71] J. Stallkamp, M. Schlipsing, J. Salmen, and C. Igel. Man vs. computer: Benchmarking machine learning algorithms for traffic sign recognition. *Neural Networks*, 32:323–332, 2012. ISSN 0893-6080. doi: <https://doi.org/10.1016/j.neunet.2012.02.016>. URL <https://www.sciencedirect.com/science/article/pii/S0893608012000457>.
- [72] George Stoica, Daniel Bolya, Jakob Brandt Bjorner, Pratik Ramesh, Taylor Hearn, and Judy Hoffman. ZipIt! Merging models from different tasks without training. In *The Twelfth International Conference on Learning Representations*, 2024. URL <https://openreview.net/forum?id=LEYUkvdUhq>.
- [73] Oyvind Tafjord, Matt Gardner, Kevin Lin, and Peter Clark. QuaRTz: An open-domain dataset of qualitative relationship questions. In *Proceedings of the 2019 Conference on Empirical Methods in Natural Language Processing and the 9th International Joint Conference on Natural Language Processing (EMNLP-IJCNLP)*, pages 5941–5946, Hong Kong, China, November 2019. Association for Computational Linguistics. doi: 10.18653/v1/D19-1608. URL <https://aclanthology.org/D19-1608/>.
- [74] Norman Tatro, Pin-Yu Chen, Payel Das, Igor Melnyk, Prasanna Sattigeri, and Rongjie Lai. Optimizing mode connectivity via neuron alignment. In *Advances in Neural Information Processing Systems*, volume 33, pages 15300–15311. Curran Associates, Inc., 2020. URL https://proceedings.neurips.cc/paper_files/paper/2020/file/aecad42329922dfc97eee948606e1f8e-Paper.pdf.
- [75] Gemini Team, Rohan Anil, Sebastian Borgeaud, Jean-Baptiste Alayrac, Jiahui Yu, Radu Soricut, Johan Schalkwyk, Andrew M Dai, Anja Hauth, Katie Millican, et al. Gemini: a family of highly capable multimodal models. *arXiv preprint arXiv:2312.11805*, 2023.
- [76] Hugo Touvron, Thibaut Lavril, Gautier Izacard, Xavier Martinet, Marie-Anne Lachaux, Timothée Lacroix, Baptiste Rozière, Naman Goyal, Eric Hambro, Faisal Azhar, Aurelien Rodriguez, Armand Joulin, Edouard Grave, and Guillaume Lample. LLaMA: Open and efficient foundation language models, 2023. URL <https://arxiv.org/abs/2302.13971>.
- [77] Alex Wang, Yada Pruksachatkun, Nikita Nangia, Amanpreet Singh, Julian Michael, Felix Hill, Omer Levy, and Samuel Bowman. Superglue: A stickier benchmark for general-purpose language understanding systems. *Advances in neural information processing systems*, 32, 2019.
- [78] Alex Wang, Amanpreet Singh, Julian Michael, Felix Hill, Omer Levy, and Samuel R. Bowman. GLUE: A multi-task benchmark and analysis platform for natural language understanding. In *International Conference on Learning Representations*, 2019. URL <https://openreview.net/forum?id=rJ4km2R5t7>.
- [79] Alex Warstadt, Amanpreet Singh, and Samuel R. Bowman. Neural network acceptability judgments. *Transactions of the Association for Computational Linguistics*, 7:625–641, 2019. doi: 10.1162/tacl_a_00290. URL <https://aclanthology.org/Q19-1040/>.
- [80] Adina Williams, Nikita Nangia, and Samuel Bowman. A broad-coverage challenge corpus for sentence understanding through inference. In *Proceedings of the 2018 Conference of the North American Chapter of the Association for Computational Linguistics: Human Language Technologies, Volume 1 (Long Papers)*, pages 1112–1122, New Orleans, Louisiana, June 2018. Association for Computational Linguistics. doi: 10.18653/v1/N18-1101. URL <https://aclanthology.org/N18-1101/>.
- [81] Mitchell Wortsman, Gabriel Ilharco, Samir Ya Gadre, Rebecca Roelofs, Raphael Gontijo-Lopes, Ari S Morcos, Hongseok Namkoong, Ali Farhadi, Yair Carmon, Simon Kornblith, and Ludwig Schmidt. Model soups: averaging weights of multiple fine-tuned models improves accuracy without increasing inference time. In *Proceedings of the 39th International Conference*

- on Machine Learning*, volume 162 of *Proceedings of Machine Learning Research*, pages 23965–23998. PMLR, 17–23 Jul 2022. URL <https://proceedings.mlr.press/v162/wortsman22a.html>.
- [82] Jianxiong Xiao, James Hays, Krista A. Ehinger, Aude Oliva, and Antonio Torralba. SUN database: Large-scale scene recognition from abbey to zoo. In *2010 IEEE Computer Society Conference on Computer Vision and Pattern Recognition*, pages 3485–3492, 2010. doi: 10.1109/CVPR.2010.5539970.
- [83] Prateek Yadav, Derek Tam, Leshem Choshen, Colin Raffel, and Mohit Bansal. TIES-merging: Resolving interference when merging models. In *Thirty-seventh Conference on Neural Information Processing Systems*, 2023. URL <https://openreview.net/forum?id=xtaX3WyCj1>.
- [84] Yi Yang, Wen-tau Yih, and Christopher Meek. WikiQA: A challenge dataset for open-domain question answering. In *Proceedings of the 2015 Conference on Empirical Methods in Natural Language Processing*, pages 2013–2018, Lisbon, Portugal, September 2015. Association for Computational Linguistics. doi: 10.18653/v1/D15-1237. URL <https://aclanthology.org/D15-1237>.
- [85] Le Yu, Bowen Yu, Haiyang Yu, Fei Huang, and Yongbin Li. Language models are super mario: absorbing abilities from homologous models as a free lunch. In *Proceedings of the 41st International Conference on Machine Learning, ICML’24*. JMLR.org, 2024.
- [86] Yuan Zhang, Jason Baldridge, and Luheng He. PAWS: Paraphrase adversaries from word scrambling. In *Proc. of NAACL*, 2019.

A Extended Related Works

Superposition and Polysemanticity in Neural Networks Multiple works cue that neural networks encode more features than available dimensions [56]. Olah et al. [55] and Nguyen et al. [53] study individual neurons in CNN models and find that neurons are polysemantic—each capable of detecting and responding to several different input patterns. Arora et al. [4] identifies that word embeddings encode different senses of polysemous words in a linear superposition fashion. Olah et al. [57] indicates that, instead of assigning each feature to one dedicated neuron, spreading a single feature across multiple neurons allows deep learning models to pack more features into the limited number of neurons they have. Elhage et al. [19] employs toy models to explore the superposition idea. They find that as input feature sparsity increases, models use superposition to represent features beyond what a linear model would typically be able to, though at the cost of compression noise that requires nonlinear filtering. Scherlis et al. [67] studies polysemanticity through the lens of allocation of limited feature capacity. They show that networks tend to represent important features monosemantically, and compress together less significant features in polysemantic way. Henighan et al. [29] then applies the toy models to establish the relationship between superposition, overfitting, and double descent.

B Limitations and Broader Impacts

B.1 Limitations and future works

As with other model merging methods, DRM may not be universally effective across all task combinations. Tasks with fundamentally conflicting objectives or disparate learned features may result in suboptimal merging performance, potentially leading to negative transfer on certain tasks. The effectiveness of DRM merged models in generalizing to entirely unseen tasks during merging remains unexplored. Our experiments were based on a variety of transformer models. However, experiments on other architecture types such as CNN and RNN remain to be explored. Furthermore, while we employ interference reduction techniques from TIES Merging [83] in our work, theoretical understanding of the merging interference and their mitigation is still limited, and we sought to answer more in the future.

B.2 Impact statement

Here, we discuss potential societal impacts of our works. Possible positive impacts are: (a) Democratization of Deep Learning: model merging lowers the barrier to entry for developing deep learning models. Pretrained and finetuned open-source models can be leveraged through merging to create custom models tailored to specific needs, fostering innovation in diverse domains. (b) Resource Efficiency: by enabling the creation of multitask models without the need for expensive retraining or joint training, DRM can significantly reduce the computational resources and energy consumption associated with training deep learning models, contributing to faster and more sustainable AI development. In contrary, our work is not tied to any one specific application, there are no obvious negative societal downside. While it might be possible that merging models with certain hidden biases inadvertently exacerbates the biases into the resulting model, this is largely dependent on the individual model being merged.

C Significance Analysis of the Merging Performance

To assess the statistical significance of the performance differences observed in Figure 2, we conducted paired t-tests between DRM-H and each of the compared baselines (Simple Averaging, TIES Merging, and DARE-TIES) for each subset size (number of tasks merged).

The results of the paired t-tests are summarized in Table 5 and 6. We report the p-values obtained for each comparison at each subset size. P-values less than 0.05 were considered statistically significant.

In ViT-B/32, as the number of tasks increases, the performance differences between DRM-H and the baselines become statistically significant, the p-values consistently fall below 0.05 starting at 3 tasks. This suggests the superior performance of DRM-H in scaling to a larger number of tasks.

Table 5: P-values from paired t-tests for each subset size on ViT-B/32. The null hypothesis assumes equal performance between DRM-H and the baselines, while the alternative hypothesis assumes DRM-H performs better.

Method	Number of tasks						
	2	3	4	5	6	7	8
Averaging	8.41e-7	1.03e-11	2.73e-14	1.33e-15	4.40e-18	6.38e-17	2.18e-3
Ties	9.96e-1	1.49e-3	1.35e-10	1.60e-12	6.69e-16	7.85e-14	4.61e-3
Dare-ties	9.99e-1	7.04e-4	9.83e-11	1.62e-13	4.45e-16	2.74e-14	3.80e-3

Table 6: P-values from paired t-tests for each subset size on T5-Base. The null hypothesis assumes equal performance between DRM-H and the baselines, while the alternative hypothesis assumes DRM-H performs better.

Method	Number of tasks				
	2	3	4	5	6
Averaging	1.68e-3	4.20e-6	1.73e-10	2.28e-7	2.83e-2
Ties	8.76e-1	3.68e-2	1.58e-2	6.72e-2	2.32e-1
Dare-ties	9.81e-1	2.23e-1	2.01e-1	1.48e-1	3.17e-1

D Theoretical Bound of Difference Between Individual Task and the Concatenated Matrix

This section theoretically evaluates the bounded difference between weight delta of each individual task, and the horizontally concatenated matrix used in DRM-H. We express the difference through their corresponding singular values (i.e. i -th singular value of a single weight delta matrix, and i -th singular value of the concatenated matrix).

We begin by stating a theorem proven by Shamrai [68]:

Lemma 1 (Singular Value Perturbation of a Concatenated Matrix Theorem in [68]). *Let $\{A_j\}_{j=1}^k$ be a collection of matrices with $A_j \in \mathbb{R}^{m \times n}$ for all $j \in [1, k]$. Define the original concatenated matrix by*

$$M = [A_1 \dots A_k] \in \mathbb{R}^{m \times kn},$$

and denote its rank by $r = \text{rank}(M)$. Let $\tilde{M} = [\tilde{A}_1 \dots \tilde{A}_k]$ be the perturbed version of M , and define the perturbation matrix

$$E = \tilde{M} - M = [E_1 \dots E_k], \quad \text{with } E_j = \tilde{A}_j - A_j \text{ for each } j \in [1, k].$$

Then, the following perturbation bounds for the singular values hold:

- For $i = 1, \dots, r$ (corresponding to the nonzero singular values of M),

$$\left| \sigma_i(\tilde{M}) - \sigma_i(M) \right| \leq \frac{1}{\sigma_i(M)} \sum_{j=1}^k (2\|A_j\|_2 \|E_j\|_2 + \|E_j\|_2^2).$$

- For $i = r + 1, \dots, \min(m, kn)$ (corresponding to the zero singular values of M),

$$\sigma_i(\tilde{M}) \leq \sqrt{\sum_{j=1}^k (2\|A_j\|_2 \|E_j\|_2 + \|E_j\|_2^2)}.$$

Then, we consider the relationship between singular value of a single matrix, compared to when it is repeatedly concatenated into a horizontal block matrix:

Proposition 1. *Suppose that $M \in \mathbb{R}^{m \times kn}$ is a horizontal concatenation of k copies of $A \in \mathbb{R}^{m \times n}$; then,*

$$\sigma_i(M) = \sqrt{k} \sigma_i(A),$$

where $\sigma_i(\cdot)$ denotes the i -th singular value.

Proof of Proposition 1. First, we consider the MM^T as a block matrix multiplication:

$$MM^T = [A \ A \ \dots \ A] \begin{bmatrix} A^T \\ A^T \\ \vdots \\ A^T \end{bmatrix} = \sum_{j=1}^k AA^T = kAA^T.$$

For an eigenvector x_i corresponding to $\lambda_i(AA^T)$, we see that

$$MM^T x_i = kAA^T x_i = k\lambda_i(AA^T)x_i.$$

This implies $\lambda_i(MM^T) = k\lambda_i(AA^T)$. By definition, the singular value of matrix M equals the square-root of the corresponding eigenvalue of MM^T :

$$\sigma_i(M) = \sqrt{\lambda_i(MM^T)} = \sqrt{k\lambda_i(AA^T)} = \sqrt{k} \cdot \sqrt{\lambda_i(AA^T)} = \sqrt{k} \cdot \sigma_i(A).$$

□

Building on the previous arguments, we hereby establish the bound:

Proposition 2. Suppose that A is an arbitrary weight delta ΔW_t , and $M \in \mathbb{R}^{m \times kn}$ is a concatenation of k copies of A , where k is the total number of tasks and r is the rank of M . Let $\widetilde{M} = [\Delta W_1 \ \dots \ \Delta W_k]$ be the concatenation of the collection $\{\Delta W_j\}_{j=1}^k$. We define the perturbation matrix

$$E = \widetilde{M} - M = [E_1 \ \dots \ E_k], \quad \text{with } E_j = \Delta W_j - A \quad \text{for each } j \in [1, k].$$

Then, the difference between i -th singular value of concatenated matrix \widetilde{M} and individual ΔW_t for all $i \in [1, r]$ and $t \in [1, k]$ is bounded by

$$|\sigma_i(\widetilde{M}) - \sqrt{k}\sigma_i(A)| \leq \frac{1}{\sqrt{k}\sigma_i(A)} \sum_{j=1}^k (2\|A\|_2 \|E_j\|_2 + \|E_j\|_2^2).$$

Proof of Proposition 2. From Lemma 1, we obtain the perturbation bound for the singular values as follows:

$$|\sigma_i(\widetilde{M}) - \sigma_i(M)| \leq \frac{1}{\sigma_i(M)} \sum_{j=1}^k (2\|A_j\|_2 \|E_j\|_2 + \|E_j\|_2^2) \quad \text{for all } i \in [1, r].$$

Then, we substitute $\sigma_i(M)$ with $\sqrt{k}\sigma_i(A)$, following Proposition 1:

$$|\sigma_i(\widetilde{M}) - \sqrt{k}\sigma_i(A)| \leq \frac{1}{\sqrt{k}\sigma_i(A)} \sum_{j=1}^k (2\|A\|_2 \|E_j\|_2 + \|E_j\|_2^2) \quad \text{for all } i \in [1, r].$$

Finally, we substitute back $A = \Delta W_t$, acquiring

$$|\sigma_i(\widetilde{M}) - \sqrt{k}\sigma_i(\Delta W_t)| \leq \frac{1}{\sqrt{k}\sigma_i(\Delta W_t)} \sum_{j=1}^k (2\|\Delta W_t\|_2 \|E_j\|_2 + \|E_j\|_2^2) \quad \text{for all } i \in [1, r].$$

□

This result quantifies the bounded behavior of change to each individual task's weight delta, such that the alteration induced by horizontal concatenation of weight deltas will never exceed a specific amount described by the bound. From this derived inequality, it is evident that larger singular values $\sigma_i(\Delta W_t)$ will exhibit a tighter bound due to the reciprocal term $\frac{1}{\sigma_i(\Delta W_t)}$ on the right hand side. The coefficient \sqrt{k} naturally arises for our DRM approach, which involves concatenating k matrices; however, this factor is generally not problematic as the number of tasks k is typically small and remains relatively consistent for each merging setting. Likewise, vertically concatenated matrices can also be bounded by going through the same steps on the transposed version, producing a very similar inequality due to the invariance under transpose property of singular value and spectral norm. We then discuss the indication of this singular value bound:

Bounded behavior of weight deltas concatenation. Intuitively, when comparing weight deltas of different models during interference mitigation, it is essential to preserve the top principle features of each model to ensure a fair comparison across tasks; otherwise, certain tasks could be degraded unknowingly. Our derived bound addresses this by indicating a bounded degree of change, especially for the important feature bases characterized by high singular values. This bound, *inherent to the properties of the concatenation process*, assures the preservation of salient information from each model, facilitating interference reduction and merging in the subsequent steps.

E Analysis of Merging through Different Decompositions

Whilst we choose to employ SVD in this work, it is natural to consider alternative decomposition techniques. This section analyzes the implication of different decompositions to our problem of model merging.

E.1 Singular Value Decomposition

One of the most widely used decomposition technique, SVD factorizes a matrix into a rotation, rescaling, and another rotation respectively. Namely, given a real matrix $A \in \mathbb{R}^{m \times n}$, we have the SVD:

$$A = U \Sigma V^T,$$

where left singular vector matrix $U \in \mathbb{R}^{m \times m}$ is a real orthogonal matrix with its column describing the column space of A , right singular vector matrix $V^T \in \mathbb{R}^{n \times n}$ is a real orthogonal matrix with its row describing the row space of A ; and singular value matrix $\Sigma \in \mathbb{R}^{m \times n}$ is a non-negative real diagonal matrix, with singular values as its diagonal entries. The number of non-zero singular values equals the rank of the matrix A .

SVD is desirable for our approach due to three key properties:

Decoupling between basis scales and directions. As demonstrated earlier, applying SVD on the concatenated weight deltas decomposes them into a matrix of shared basis (U), a scaling matrix (Σ), and individual basis matrices (V_t^T) that are aligned inside the same shared space. The decoupling of directions captured by singular vectors, and scales captured by singular values, grants us the ability to work on the feature direction and magnitude separately. Allowing us to organize our DRM algorithm as proposed in Section 4: (1) pruning the scale-less basis vector matrices, then (2) performing sign election and disjoint averaging on the scaled basis vector matrices. See matrix depiction of our method in Figure 4.

Invariance of concatenation orders. Different orders of weight delta concatenation: $[A \ B]$ and $[B \ A]$ should produce the same shared space represented by U (or very similar in practice). This invariance is crucial in ensuring the robustness of the decomposition process. As we treat each task as equal peers, shuffling the task concatenation order should not generate different merging outcomes.

Factorization into column and row basis matrices. This enables us to meaningfully concatenate the weight deltas in either horizontal (DRM-H) or vertical (DRM-V) direction, analogous to decomposing into a shared column or row space respectively. We discuss the implications and distinctions between the twos thoroughly in Section G.

Moreover, the sorted singular value property of SVD also enables direct manipulation of matrix rank. Low-rank approximation can be obtained simply by zeroing out smaller singular value entries [17]. However, this property was not utilized in DRM as we observed that dropping rank leads to decrease in performance (Section H.1).

While SVD offers numerous benefits, it also has limitations. First of all, SVD is computationally more intensive compared to other matrix decompositions, and can become a bottleneck as the sizes of the weight delta matrices grow. We mitigate this by running SVD on a GPU via the cuSOLVER library. Furthermore, SVD is non-unique. Namely, multiplying both a left singular vector u_i and its corresponding right singular vector v_i by -1 yields another valid SVD. This non-uniqueness arises because SVD identifies a *subspace* of the matrix, not the exact feature, and the sign of basis vectors can flip without effecting the space. However, this is not problematic for our use case. In DRM-H, as

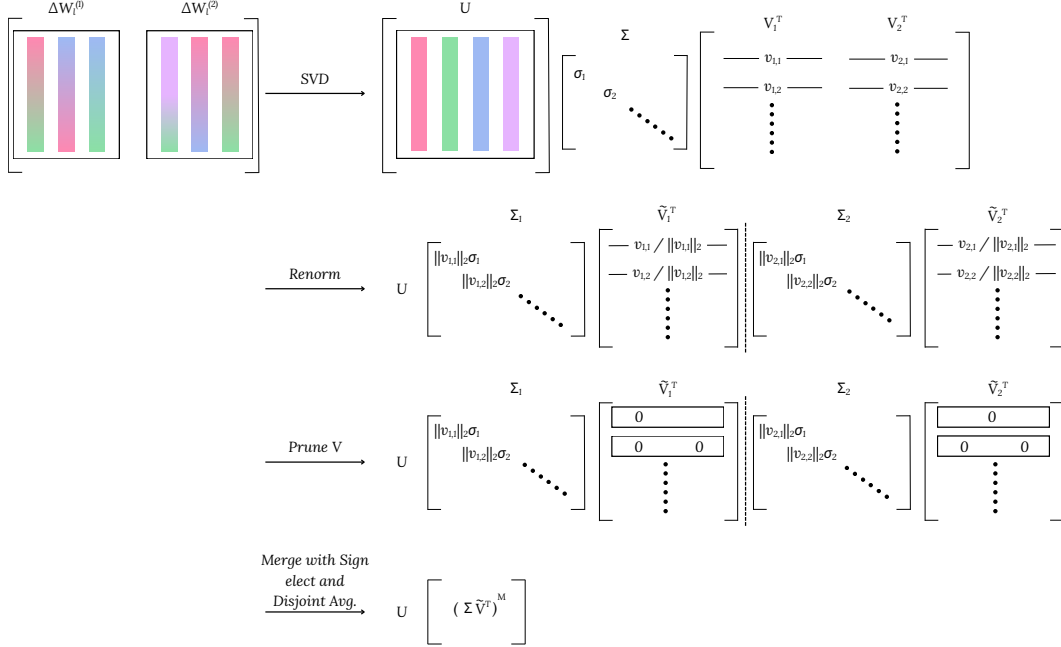


Figure 4: A matrix viewpoint of DRM-H. **(First row)** Horizontal joint decomposition. **(Second row)** Renormalization on row basis vectors. **(Third row)** Pruning of the right singular vector matrices. **(Fourth row)** Sign election and disjoint averaging of right singular vector matrices.

U is always shared across weight deltas, if a single column u_i is sign flipped, then row basis $v_{t,i}$ of every task will also be flipped, leading to no net effect in downstream sign election. The same holds for DRM-V.

Here is one simple illustration of the non-uniqueness of SVD. Let $A = \begin{bmatrix} 1 & 0 \\ 0 & 2 \end{bmatrix}$, a valid SVD is $\begin{bmatrix} 1 & 0 \\ 0 & 1 \end{bmatrix} \begin{bmatrix} 1 & 0 \\ 0 & 2 \end{bmatrix} \begin{bmatrix} 1 & 0 \\ 0 & 1 \end{bmatrix}$. Another valid SVD is obtained by flipping the sign of the second singular vector: $\begin{bmatrix} 1 & 0 \\ 0 & -1 \end{bmatrix} \begin{bmatrix} 1 & 0 \\ 0 & 2 \end{bmatrix} \begin{bmatrix} 1 & 0 \\ 0 & -1 \end{bmatrix}$.

E.2 QR Decomposition

The QR decomposition factorizes a matrix into a set of column basis vectors, and their column operations. Namely, given a matrix $A \in \mathbb{R}^{m \times n}$, we have the QR decomposition:

$$A = QR,$$

where $Q \in \mathbb{R}^{m \times m}$ is an orthogonal matrix, and $R \in \mathbb{R}^{m \times n}$ is an upper triangular matrix.

Similar what we have done with the SVD, we can apply the QR decomposition to the horizontally concatenated weight deltas, and view the step as aligning into a shared column space described by Q . Notwithstanding, *QR decomposition is strongly dependent to the ordering of columns*, and by extension, strongly dependent to the order of weight deltas concatenation. The first column of Q will always be the normalized first column of A (or negative counterpart of the same normalized vector), due to the upper triangular constraint of R . Additionally, if we were to mimic the step of splitting V^T into $\{V_t^T\}_{t=1}^N$ in DRM for representing each model, splitting R produces submatrices $\{R_t\}_{t=1}^N$ with imbalanced distribution of zero entries due to the triangular structure of R . These behavior could introduce bias in the subsequent interference reduction and merging steps.

E.3 Canonical Polyadic Decomposition

While joint decomposition through SVD effectively establishes a shared representation space for interference reduction and merging, 2-dimensional structure of matrix may not fully capture the complex interdependencies between models being merged. We briefly explore the use of Canonical Polyadic (CP) decomposition, a tensor factorization technique that can potentially model higher-order interactions across multiple models.

CP decomposition factorizes a tensor into a sum of k rank-one tensors [42]. For our application, we can stack p weight delta matrices in a new axis, forming a tensor $\mathcal{T} \in \mathbb{R}^{p \times m \times n}$. We have the CP decomposition:

$$\mathcal{T} = \sum_{r=1}^R \lambda_r (\mathbf{a}_r \otimes \mathbf{b}_r \otimes \mathbf{c}_r)$$

where R is the rank of the CP decomposition, λ_r is the scaling factor of the r -th rank. $\mathbf{a}_r \in \mathbb{R}^p$, $\mathbf{b}_r \in \mathbb{R}^m$, and $\mathbf{c}_r \in \mathbb{R}^n$ are the factor vectors for the r -th component. The symbol \otimes denotes the Kronecker product. Each rank-one tensor represents a basis component of the overall tensor, capturing a specific pattern of interaction between weight deltas.

In principle, we could adapt DRM to work with the CP decomposition. Analogously, we could partition the factor vector \mathbf{a}_r into p segments, each representing the contribution of a single model to the r -th component. Then, we multiply the segment back with other two corresponding factor vectors of the r -th rank, and apply interference reduction and merging techniques to these segments in the shared CP space.

However, we encounter significant obstacles with this approach, primary of which is the inherent computation burden of CP decomposition. In our experiments using TensorLy [43], merging through CP decomposition took up hours on even our smallest model ViT-B/32. Determining the rank of a tensor is also NP-hard [31], demanding tuning search to find the optimal rank hyperparameter.

F Elaboration of Sign Agreement Analysis

Already investigated in Section 6.2, using sign agreement as a measure of interference. Here we compliment the previous investigation, and visualize detailed histograms comparing the distribution of sign agreements after pruning the original and the Decompose-renormalized spaces of ViT-B/32 and Llama3.1-8B, in Figure 5.

Particularly, for the histogram labels *Horizontal* and *Vertical*, we first project the weight deltas into the Decompose-renormalized space, apply pruning to the basis vector entries, and measure the sign agreements. Afterwards, we transform the results back to the original space and measure sign agreement, labeled *Horizontal (Original Space)* and *Vertical (Original Space)*. For the histogram label *Original Weight*, we simply directly prune the weight deltas and report their sign agreements.

Note that that the minimum sign agreement is 50%, when there are an equal numbers of positive and negative entries. Notably, for the bin of 0.9 – 1.0 sign agreement level, transforming back to the original space showcases a sign agreement drop of approximately 3 folds, on both models we experimented on. This supports our conclusion in Section 6.2.

G Horizontal vs. Vertical Joint Decomposition

This work introduces two variants of DRM: (1) *DRM-H*, which performs joint decomposition on horizontally concatenated weight deltas, and (2) *DRM-V*, which operates on vertically concatenated weight deltas. These processes can be interpreted as decomposing and coordinating weight deltas into a shared column space (DRM-H) or a shared row space (DRM-V). Empirically, we observe that DRM-H demonstrated a superior performance over DRM-V across all settings evaluated without hyperparameter tuning, including ViT-B/32, ViT-L/14, DeBERTa-Base, T5-Base, T5-Large, and Llama3.1-8B (with a surplus as large as 12.8% in DeBERTa-Base). On the other hand, when held-out validation set was available for tuning, DRM-V managed to achieve higher performance compared to DRM-H on T5-Base, T5-Large, and Llama3.1-8B (0.7%, 2.3%, and 1.0% absolute improvements, respectively). This suggests that DRM-H is generally more robust and outperforms DRM-V across a

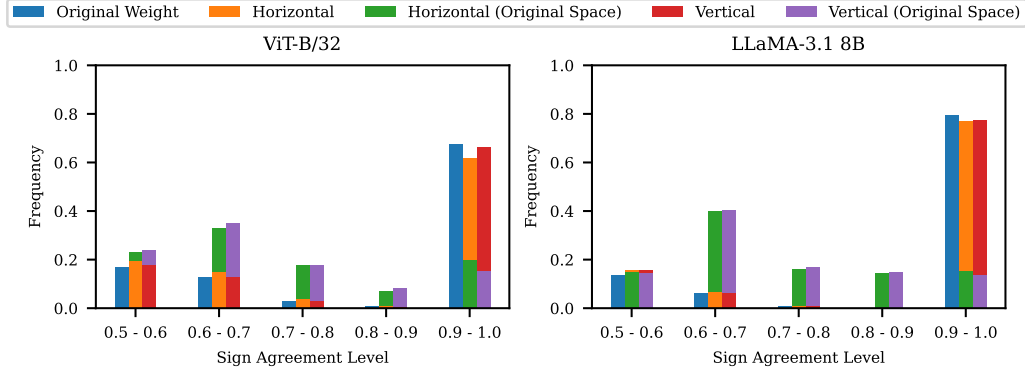


Figure 5: Histogram of sign agreement after pruning the original and the Decompose-renormalized spaces of ViT-B/32 and LLaMA-3.1 8B. For each position in the weight delta matrix, we tally the agreement in sign across different tasks. Then, the agreement across all positions are aggregated into a histogram. The range of sign agreement is between 0.5 and 1.0, where 0.5 denotes a position that has an equal number of positive and negative values, while 1.0 refers to a position where all tasks have the same sign. We visualize the sign agreement in original parameter space (*blue*), the joint singular space (*orange* and *red*), and after projecting joint singular space back to the original space (*green* and *purple*).

wide range of merging settings. While DRM-V may be more sensitive to hyperparameter settings, it can occasionally achieve higher performance on specific models and tasks with careful tuning.

One possible consideration for the two variants concerns the shape of the weight matrices. While many linear transformations within the self-attention mechanism of transformers utilize square matrix, certain models employ rectangular projection weights. For example, models using Grouped Query Attention [2], such as Llama3.1-8B [76, 24] used in our experiments, often adopt rectangular key and value projection weights with more columns than rows. This difference in input and output dimensionality results in different effective dimension of the Decompose-renormalized space for us to work on. Concretely, for weight deltas of shape $m \times n$, DRM-H aligns weight deltas into a shared column space, and work on the partitioned row basis vectors of dimension n , while DRM-V aligns the deltas into a mutual row space, and work on the partitioned column basis vectors of dimension m . Due to *frequent orthogonality* property of high dimensional space, vectors are much more likely to be orthogonal in higher dimensions. Prior work Ilharco et al. [35] speculated that higher orthogonality between task vectors corresponds to lower interference during model merging. Given this, if $m \neq n$, then the disparate degree of orthogonality between basis vectors could be a source of the observed differences in merging outcomes between DRM-H and DRM-V.

Additionally, model architectures and training schemes seem to play a role as well. As we observe that DRM-H consistently exceeds DRM-V’s performance when merging encoder-based models: ViT-B/32, ViT-L/14, DeBERTa-Base. Then, DRM-V outperforms when performing tuned merging on encoder-decoder-based and decoder-only models: T5-Base, T5-Large, and Llama3.1-8B. We leave in-depth study of the effect and connection between DRM-H and DRM-V as future work.

H Additional Experiments and Results

H.1 Effect of rank truncation

Given that SVD employed in DRM factorizes the concatenated weight deltas into a spectrum of singular values, it is natural to consider the effect of rank truncation for the possibility of further parameter interference reduction and improved merging performance. We explore dropping small singular values (i.e. correspond to dropping less important singular vectors) to demonstrate the effect of rank truncation. After applying SVD to $\Delta W_l^{\text{stack}}$, we retain only the top $(1 - k) \cdot r$ ranks, where r is the rank of $\Delta W_l^{\text{stack}}$, and k is the rank drop rate; before proceeding with the merging procedure. As show in Figure 6, the performance remains relatively stable, and only begins to

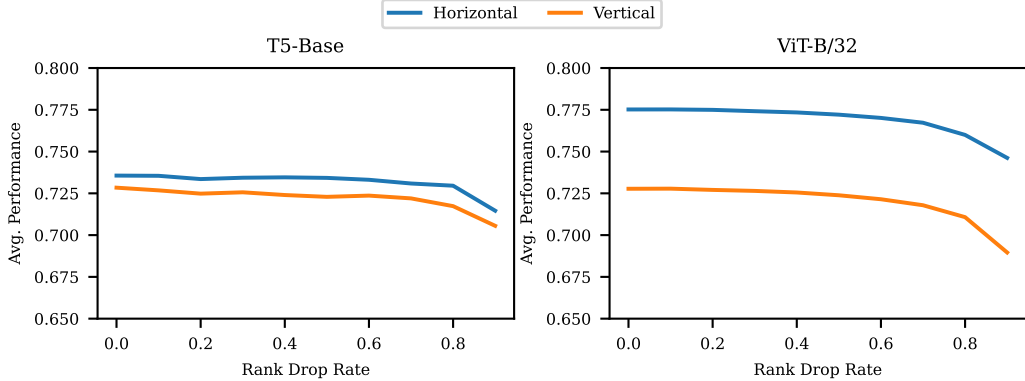


Figure 6: Performance of T5-Base and ViT-B/32 when dropping small singular values. A rank drop rate of k means retaining only the top $(1 - k)$ portion of the singular values before renormalization (multiplying vector norms back into the singular values during renormalization could cause changes in singular value ordering). We see that the performance remains relatively stable, with only a slight decreasing trend. The performance only begins to degrade noticeably after k is greater than 0.8.

degrade noticeably after k is greater than 0.8. However, as truncating ranks does not result in distinct performance increment, we did not employ this procedure in DRM. The absence of improvements may indicate that the lower-ranked singular vectors, while contributing less individually, still capture valuable information; or that the interference caused by these components is negligible. Future work could explore alternative methods in manipulating the less important singular vectors for potential interference reduction.

H.2 Ablation of interference reduction components

To evaluate the contribution of each interference reduction technique [83] employed in DRM-H, we perform an ablation analysis by removing each component individually and evaluate the resulting performance. We remove: (1) pruning (2) sign election (3) disjoint averaging (replaced with simple averaging). Table 7 shows the results of this analysis.

We recognize that disjoint averaging is the most critical component of DRM-H, removing this technique causes significant performance drops in both ViT-B/32 and T5-Base up to 16.1% absolutely. Surprisingly, we also find that merging without sign election improves the merging performance by 3.1% on T5-Base, this result warrants further investigation in future work.

Table 7: Ablation of interference reduction techniques employed in DRM-H

Method	ViT-B/32	T5-Base
DRM-H	77.5	73.6
- Prune	74.9	72.4
- Elect Sign	76.6	76.7
- Disjoint Average	62.9	57.5

H.3 Justification of joint pruning

In the pruning step, two possible approaches can be made: (1) joint pruning: concatenate singular vector matrices (i.e. \tilde{V}_t for DRM-H and \tilde{U}_t for DRM-V) across all tasks before sorting the entries for top- $k\%$ and then prune the rest. (2) individual pruning: prune each singular vector matrix separately. To justify our design choice, we summarize the comparison between these two approaches in Table 8.

In ViT-B/32 and T5-Base, the performances between joint and individual pruning are comparable, with joint pruning performing slightly better or equal for both DRM-H and DRM-V. On the other hand, DeBerta-Base is more sensitive, with joint pruning achieving 0.9% absolute improvement compared to individual pruning when merging with either DRM-H or DRM-V. Motivated by the improvement, our method employs joint pruning.

Table 8: Comparison of merging results with joint and individual pruning.

Method	Trim	ViT-B/32	T5-Base	DeB-Base
DRM-H	Individual	77.4	73.6	66.0
	Joint	77.5	73.6	66.9
DRM-V	Individual	72.8	72.5	53.2
	Joint	72.8	72.8	54.1

H.4 Hyperparameter sensitivity

To assess the robustness of DRM, we conduct a sensitivity analysis to evaluate how the performance of merging techniques varies with different hyperparameter settings, when merging ViT-B/32, T5-Base, and Llama3.1-8B. We focus on two hyperparameters: (1) Pruning retention rate k . (2) Merging Coefficient λ .

We report the result in Figure 7. The analysis suggests that DRM is generally more robust to hyperparameter variations within a reasonable range, compared to TIES Merging and DARE-TIES, especially when merging ViT-B/32 and T5-Base, but careful tuning is still crucial for enhancing the merging results. This information can guide future selection of appropriate hyperparameter values for DRM. *The accuracy reported here were measured on validation set*, reflecting the hyperparameter tuning search.

H.5 Hyperparameter tuning

To ensure fair and optimal comparisons, we report in Section 5 both merging performance on default hyperparameters, and performance using hyperparameters tuned via grid search on held-out validation sets described in Section I. This section details the hyperparameter search spaces.

For each merging technique, we tuned the following hyperparameters:

- **Task Arithmetic:** The merging coefficient λ .
- **TIES Merging:** Prune rate, and merging coefficient λ .
- **DARE-TIES:** Prune rate, and merging coefficient λ .
- **DRM-H & DRM-V:** Prune rate, and merging coefficient λ .

Following Ilharco et al. [35], Ortiz-Jimenez et al. [59], every method uses a single merging coefficient λ value shared across every task.

For Task Arithmetic, we explored a merging coefficient search space $\lambda \in \{0.1, 0.2, 0.3, \dots, 1.0\}$. For TIES Merging, DARE-TIES, DRM-H and DRM-V, we specify the search space for merging coefficient $\lambda \in \{0.8, 0.9, 1.0, \dots, 1.5\}$; and prune rate $k \in \{0.1, 0.2, 0.3, \dots, 1.0\}$, the range is selected to be exhaustive regardless of whether the pruning is defined by prune rate or retention rate. Notice that the Task Arithmetic employs λ as a coefficient for weighted sum, while other methods utilize λ on top of averaging. Therefore, their search spaces cover different scales.

H.6 Per-task performance breakdown

To provide a more detailed analysis of the performance of our proposed DRM method, this section presents a breakdown of the results for each individual task in our evaluation suite. Complementing the aggregate performance presented in Section 5. All the reported results are classification accuracy.

Specifically, refer to

- Table 10 for per-task performance of ViT-B/32,
- Table 11 for per-task performance of ViT-L/14,
- Table 12 for per-task performance of T5-Base,
- Table 13 for per-task performance of T5-Large,

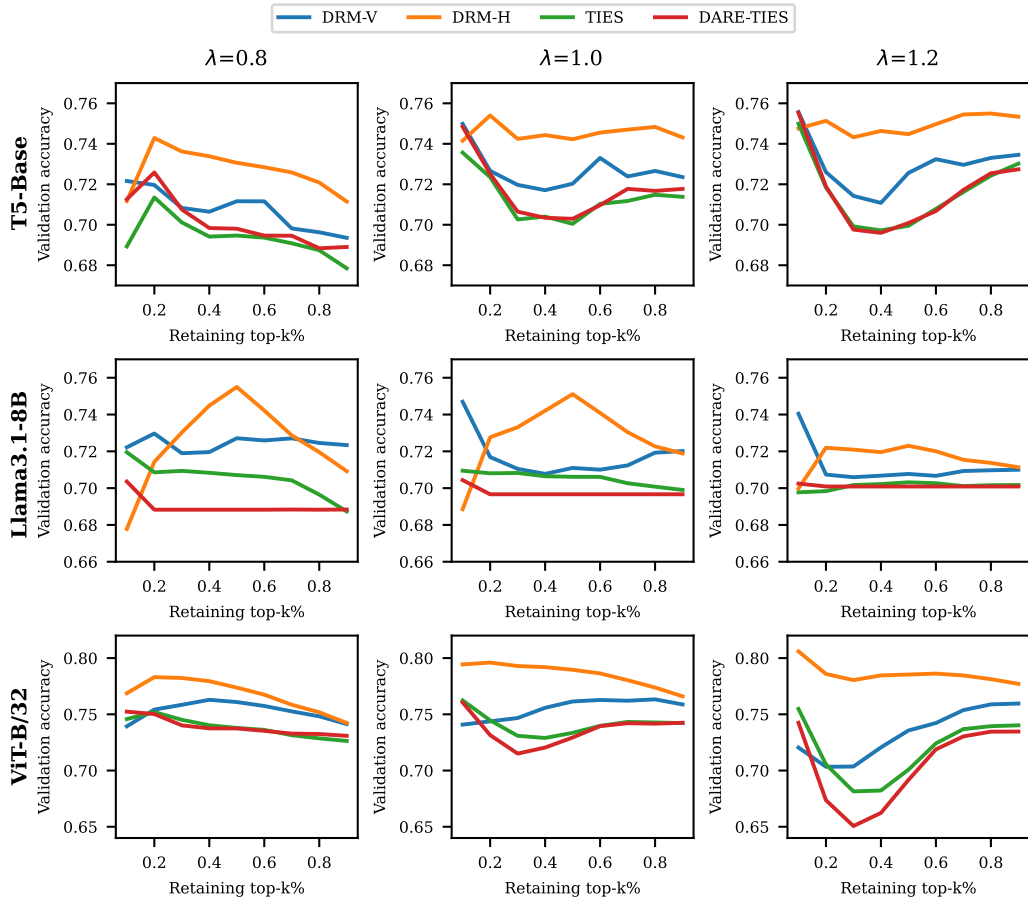


Figure 7: Hyperparameter sensitivity when merging ViT-B/32, T5-Base, and Llama3.1-8B. We fix merging coefficient λ to one of $\{0.8, 1.0, 1.2\}$, and try varying the parameter retention rate k (inverse of pruning rate). We see that the performance of both DRM-H and DRM-V is generally more robust to hyperparameter variations within a reasonable range, compared to TIES Merging and DARE-TIES. Validation set accuracy is reported here, to reflect the hyperparameter tuning search.

- Table 14 for per-task performance of DeBERTaV3-Base,
- Table 15 for per-task performance of Llama3.1-8B.

I Training Details

I.1 Vision Models

Vision models employed in our study are CLIP ViT-B/32 and CLIP ViT-L/14, each with a linear classification head attached for each task. Both the models and classifiers were provided by Ilharco et al. [35]³. The checkpoints follow the OpenCLIP implementation [34], where the self-attention’s query, key, and value projection weights are stacked into a single weight matrix. We found no discernible performance difference on applying our method to the stacked QKV versus each projection weight separately. Hence, we apply our methods on the stacked matrix to keep the implementation straightforward.

³https://github.com/mlfoundations/task_vectors

I.1.1 Datasets

For vision tasks, we used the following datasets: MNIST [45] under Gnu General Public License. EuroSAT [28] under MIT License. Cars [44] and GTSRB [71] under Creative Commons License. We could not find the license information of DTD [13], RESISC45 [11], SUN397 [82] and SVHN [52]. We attempted to reproduce the exact splits for EuroSAT and RESISC45 from Ilharco et al. [35] but were unable to do so, and instead followed the dataset sizes reported in that work.

I.2 Language Models

We chose the two variants of encoder-decoder models T5-Base⁴ and T5-Large⁵, as well as another encoder-only model DeBERTaV3-Base⁶.

I.2.1 Finetuning hyperparameters

The model were finetuned through Hugging Face’s Transformers library (*-ForSequenceClassification* class family), using the AdamW [49] optimizer with a learning rate of 1e-4, a batch size of 1024 samples, and a maximum of 50,000 optimization steps with early stopping enabled. Following Yadav et al. [83], we did not use learning rate scheduling and weight decay in our experiments, as they could introduce additional confounding factors. Bfloat16 precision was enabled for better training efficiency. A single A100 80GB GPU was used for training.

I.2.2 Datasets

We employed a diverse set of datasets, covering a range of natural language understanding tasks. Datasets were accessed via Hugging Face’s Datasets. For datasets where validation sets were not provided, we split 10% of the training set with random seed 0 to create a validation set. The following datasets were used:

PAWS[86]⁷: we used the original *labeled* split.

QASC[40]⁸: with CC-BY 4.0 license. We used a total of 8,134 training samples, 926 validation samples, and 920 test samples.

QuARTz[73]⁹: with CC-BY 4.0 license. We used the original split.

StoryCloze[51]¹⁰ comes with *2016* and *2018* splits. We used validation set of *2018* split for training, and leave the *2016* validation and test sets as they are.

WikiQA[84]¹¹: we used the original split.

WinoGrande[66]¹²: we used the *winogrande_l* training split, and partition 10% of it for validation. The original validation set was used for test instead. The final split consisted of 9,210 training samples, 1,024 validation samples, and 1,267 test samples.

Moreover, we attempted with finetuning on WSC [46], using the *wsc.fixed* subset of the SuperGLUE benchmark [77]. We tried splitting the training set to create a held-out validation set. However, we failed to train WSC models to convergence, so they were not included in our experiments.

⁴<https://huggingface.co/google-t5/t5-base>

⁵<https://huggingface.co/google-t5/t5-large>

⁶<https://huggingface.co/microsoft/deberta-v3-base>

⁷<https://huggingface.co/datasets/google-research-datasets/paws>

⁸<https://huggingface.co/datasets/allenai/qasc>

⁹<https://huggingface.co/datasets/allenai/quartz>

¹⁰https://huggingface.co/datasets/LSDSem/story_cloze

¹¹https://huggingface.co/datasets/microsoft/wiki_qa

¹²<https://huggingface.co/datasets/allenai/winogrande>

I.3 Large Language Models

For LLMs, we finetuned Llama3.1-8B¹³ using the *LlamaForSequenceClassification* class from Hugging Face’s Transformers library. Due to the high cost of training LLMs, we opted for LoRA [33] through the PEFT library, instead of full finetuning.

I.3.1 Finetuning Hyperparameters

The models were finetuned with a low learning rate of $3e-5$, and a $1e-5$ weight decay (we observed that using no weight decay at all hurts the finetuned performance considerably) via the AdamW optimizer. The training was done in a distributed fashion with an effective batch size of 256 samples, limited to a maximum of 2,000 total steps, with early stopping enabled, 5% learning rate warm up steps, and 1024 tokens context length. We applied LoRA adapters with rank 16 to every linear layer of the self-attention modules, and set the alpha to 32. Bfloat16 datatype was used together with Flash-Attention2 [14] in order to minimize memory usage and speed up the training cycles. Additional performance enhancements included the use of Liger kernel [32] and PyTorch’s *compile* utility. We conducted the training using 4 A100 GPUs, each with 80 GBs of VRAM.

I.3.2 Datasets

We evaluated our approach on the following datasets from the GLUE benchmark [78]: QNLI¹⁴, MNLI¹⁵, RTE¹⁶, SST-2¹⁷, and CoLA¹⁸, chosen to cover a range of natural language understanding tasks. Since every dataset here lacks publicly available test labels, we used the original validation sets for testing, and created new validation splits by reserving 10% of the training data, except for SST-2 and CoLA, which use only 5%, using stratified sampling with a fixed random seed of 0. The dataset statistics are summarized in Table 9.

Table 9: LLM Dataset Statistics

Dataset	Task	Training Size	Validation Size	Test Size
QNLI [78]	Question-Answering	94,268	10,475	5,463
MNLI [80]	Natural Language Inference	353,431	39,271	9,815
RTE [78]	Textual Entailment	2,241	249	277
SST-2 [70]	Sentiment Analysis	63,981	3,368	872
CoLA [79]	Linguistic Acceptability	7,695	856	1,043

¹³<https://huggingface.co/meta-llama/Llama-3.1-8B>

¹⁴<https://huggingface.co/datasets/nyu-ml/glue/viewer/qnli>

¹⁵<https://huggingface.co/datasets/nyu-ml/glue/viewer/mnli>

¹⁶<https://huggingface.co/datasets/nyu-ml/glue/viewer/rte>

¹⁷<https://huggingface.co/datasets/nyu-ml/glue/viewer/sst2>

¹⁸<https://huggingface.co/datasets/nyu-ml/glue/viewer/cola>

Table 10: Break down of ViT-B/32 merging performance.

Methods	Validation	Datasets								Average
		Cars	DTD	EuroSAT	GTSRB	MNIST	RESISC45	SUN397	SVHN	
Finetuned		77.7	79.6	99.7	98.7	99.7	98.5	75.0	97.5	90.8
Simple Averaging	×	63.4	50.4	72.8	52.8	87.5	72.5	65.0	64.1	66.1
Task Arithmetic	×	40.9	42.8	65.3	66.0	98.1	54.3	36.5	80.6	60.6
TIES Merging	×	58.8	54.3	78.6	72.1	98.3	72.4	59.4	86.2	72.5
Dare-TIES	×	55.8	52.8	78.3	71.3	98.4	69.6	56.4	86.3	71.1
DRM-H	×	64.7	59.7	89.3	75.9	98.7	81.8	65.8	84.4	77.5
DRM-V	×	56.1	53.6	80.0	74.5	98.5	73.9	59.0	86.4	72.8
Task Arithmetic	✓	62.0	52.1	78.3	64.9	94.0	73.4	63.5	74.4	70.3
TIES Merging	✓	61.8	57.1	75.1	73.1	98.4	77.6	63.8	87.3	74.3
Dare-TIES	✓	63.9	56.6	76.0	72.2	97.8	78.3	65.6	85.1	74.4
DRM-H	✓	65.4	60.6	87.4	76.3	99.0	83.1	67.1	87.8	78.3
DRM-V	✓	62.8	55.0	83.2	74.5	98.3	75.1	62.6	85.8	74.6

Table 11: Break down of ViT-L/14 merging performance.

Methods	Validation	Datasets								Average
		Cars	DTD	EuroSAT	GTSRB	MNIST	RESISC45	SUN397	SVHN	
Finetuned		92.3	84.4	99.9	99.2	99.7	99.0	81.9	98.1	94.3
Simple Averaging	×	81.6	62.7	91.1	70.6	97.0	83.7	71.9	78.2	79.6
Task Arithmetic	×	79.2	64.3	90.5	86.6	99.1	85.6	72.3	89.2	83.4
TIES Merging	×	84.9	68.8	95.3	83.3	99.0	91.2	76.1	90.3	86.1
Dare-TIES	×	84.3	68.2	95.0	83.6	99.1	90.8	75.8	90.6	85.9
DRM-H	×	86.7	71.9	96.5	89.3	99.2	93.4	76.3	90.7	88.0
DRM-V	×	83.6	68.3	95.5	86.5	99.2	90.6	75.3	91.3	86.3
Task Arithmetic	✓	82.1	65.8	93.1	86.8	98.9	88.1	73.8	87.9	84.6
TIES Merging	✓	85.8	70.6	95.1	84.1	99.2	91.9	76.7	91.5	86.9
Dare-TIES	✓	85.7	70.2	95.2	84.5	99.1	91.9	76.6	91.3	86.8
DRM-H	✓	87.8	75.2	96.6	91.9	99.2	94.7	77.1	91.6	89.3
DRM-V	✓	84.0	67.1	95.9	87.5	99.2	90.4	75.1	91.9	86.4

Table 12: Break down of T5-Base merging performance.

Methods	Validation	Datasets						Average
		PAWS	QASC	Quartz	StoryCloze	WikiQA	WinoGrande	
Finetuned		94.9	99.5	75.0	86.1	96.0	59.0	85.1
Simple Averaging	×	58.9	54.8	54.6	65.2	95.3	51.2	63.3
Task Arithmetic	×	84.1	90.6	59.7	72.6	95.1	56.6	76.4
TIES Merging	×	87.1	63.9	63.4	63.7	95.3	57.2	71.8
Dare-TIES	×	87.2	65.7	63.7	63.9	95.1	58.3	72.3
DRM-H	×	87.8	74.1	59.2	67.8	95.2	57.3	73.6
DRM-V	×	87.5	75.1	60.8	61.9	95.0	56.7	72.8
Task Arithmetic	✓	84.1	90.6	59.7	72.6	95.1	56.6	76.4
TIES Merging	✓	87.6	71.5	63.3	67.0	95.2	57.8	73.7
Dare-TIES	✓	86.8	77.2	63.3	68.0	95.2	57.2	74.6
DRM-H	✓	87.1	78.2	60.2	67.0	95.3	58.6	74.4
DRM-V	✓	86.8	88.7	61.5	62.5	95.0	56.3	75.1

Table 13: Break down of T5-Large merging performance.

Methods	Validation	Datasets						Average
		PAWS	QASC	Quartz	StoryCloze	WikiQA	WinoGrande	
Finetuned		94.5	99.5	86.2	90.4	96.0	69.0	89.3
Simple Averaging	×	79.6	73.1	66.7	69.6	95.3	55.0	73.2
Task Arithmetic	×	82.1	93.3	71.4	77.5	93.0	63.3	80.1
TIES Merging	×	83.5	63.2	65.1	64.7	91.6	65.9	72.3
Dare-TIES	×	83.9	62.8	65.4	65.0	91.4	65.4	72.3
DRM-H	×	86.0	73.1	66.6	63.1	93.5	64.6	74.5
DRM-V	×	86.4	68.7	62.8	63.0	93.5	65.3	73.3
Task Arithmetic	✓	82.1	93.3	71.4	77.5	93.0	63.3	80.1
TIES Merging	✓	82.6	91.4	71.2	73.7	92.5	65.8	79.5
Dare-TIES	✓	83.1	91.2	70.7	73.4	92.9	65.7	79.5
DRM-H	✓	85.2	72.7	67.7	67.0	93.5	64.5	75.1
DRM-V	✓	85.2	86.8	65.9	68.6	93.1	64.8	77.4

Table 14: Break down of DeBERTa-Base merging performance.

Methods	Validation	Datasets						Average
		PAWS	QASC	Quartz	StoryCloze	WikiQA	WinoGrande	
Finetuned		94.5	99.4	90.6	52.2	94.7	68.9	83.4
Simple Averaging	×	53.4	18.5	75.3	49.7	94.7	54.2	57.6
Task Arithmetic	×	45.1	25.5	73.6	49.2	83.2	55.5	55.4
TIES Merging	×	50.2	47.7	62.3	51.1	26.9	54.0	48.7
Dare-TIES	×	49.1	46.3	60.6	51.2	23.4	53.5	47.3
DRM-H	×	84.0	58.6	77.4	51.4	72.4	57.3	66.9
DRM-V	×	61.7	44.0	55.1	53.5	56.0	54.3	54.1
Task Arithmetic	✓	50.3	26.8	77.2	49.7	88.7	55.8	58.1
TIES Merging	✓	56.6	36.2	71.7	49.5	71.5	57.7	57.2
Dare-TIES	✓	57.7	34.9	71.6	50.3	73.9	58.5	57.8
DRM-H	✓	84.3	55.1	76.2	51.4	84.9	55.4	67.9
DRM-V	✓	76.6	50.9	55.9	51.5	81.7	50.3	61.1

Table 15: Break down of Llama3.1-8B merging performance.

Methods	Validation	Datasets					Average
		COLA	SST2	MNLI	QNLI	RTE	
Finetuned		83.4	96.6	91.4	95.2	85.9	90.5
Simple Averaging	×	72.8	61.9	47.5	61.0	64.3	61.5
Task Arithmetic	×	43.8	49.8	33.1	50.7	52.4	45.9
TIES Merging	×	70.7	51.4	76.5	53.5	83.4	67.1
Dare-TIES	×	70.1	51.2	79.1	51.9	85.9	67.6
DRM-H	×	72.1	55.7	71.5	63.4	84.8	69.5
DRM-V	×	70.1	51.2	85.2	53.2	85.9	69.1
Task Arithmetic	✓	69.1	50.9	80.8	50.5	80.5	66.4
TIES Merging	✓	72.7	51.8	81.0	56.2	85.6	69.4
Dare-TIES	✓	69.6	50.9	86.3	50.6	86.6	68.8
DRM-H	✓	73.2	63.1	74.7	70.7	84.8	73.3
DRM-V	✓	73.9	68.5	74.3	75.9	79.1	74.3